Sensitivity analysis of a minimum lateral control speed prediction system

Using a Fokker 50 simulation model

F. Bouwman

April 30, 2020

Technische Universiteit Delft

TU Delft

Sensitivity analysis of a minimum lateral control speed prediction system

Using a Fokker 50 simulation model

by

F. Bouwman

to obtain the degree of Master of Science
at the Delft University of Technology,
to be defended publicly on Tuesday May 12, 2020 at 13:00 PM.

Student number:	4371038	
Project duration:	March 24, 2019 – May 12, 2020	
Thesis committee:	Prof. dr. ir. M. Mulder,	TU Delft, Chair
	Ir. O. Stroosma,	TU Delft, Supervisor
	Dr. ir. A. in't Veld,	TU Delft, Supervisor
	Dr. ir. R. Vos	TU Delft, Examiner

This thesis is confidential and cannot be made public until May 12, 2020.

TU Delft

Preface

This thesis is written in fulfillment of the graduation procedure at the section of Control and Simulation (C&S) at the Aerospace Engineering department of Delft University of Technology. The subject of this thesis is inspired by the work of H. Koolstra, who wrote his PhD thesis on preventing aircraft loss of control in 2017. During his research he noticed that the C&S section lacked a validated simulation model of a twin-turboprop aircraft with asymmetric thrust functionalities. Through a contact at Fokker, he found out that Fokker owns a certified simulation model of the Fokker 50 based on extensive flight test data. This prompted my internship at Fokker Services B.V. in September 2018, during which I converted the simulation model to the software environment of C&S (DUECA). The internship was carried out under the supervision of D. van Os, who remained involved with this project as well. This project was initiated after my internship in April 2019, with the intention to carry on with the work of H. Koolstra using the Fokker 50 simulation model.

This document contains the paper that was published after the graduation project, as well as a description of additional activities that were carried out during this research project in separate appendices.

I would like to express my gratitude towards Ir. O. Stroosma and Dr. ir. A. in't Veld for their daily supervision, their help in guiding me through the graduation procedure and for sharing their knowledge on flight simulation and flight dynamics. Furthermore, I would like to thank Dr. H. Koolstra for inspiring this research and for explaining the results of his research. Finally I would like to thank Ing. D. van Os for his continued support of the Fokker 50 simulation model project, by providing extra documentation and validation data for debugging purposes.

F. Bouwman
Delft, April 30, 2020

Cover image retrieved from: https://www.youtube.com/watch?v=umhL80n5RhU

Contents

Sensitivity analysis of a minimum lateral control speed prediction system

F. Bouwman
Control & Simulation, Delft University of Technology

April 30, 2020

Abstract

Preventing Loss of Control In-flight (LOC-I) in commercial and general aviation is an active research area with numerous proposed solutions. One of these solutions aims to prevent lateral LOC-I, a special type of LOC-I, by presenting a roll-performance based minimum lateral control speed to the pilot in roll-limited situations, such as single-engine failure scenarios in multi-engine aircraft. This minimum lateral control speed is predicted by a system, named the V_c Prediction System (VPS), which continually predicts the minimum lateral control speed V_c at which an aircraft can still obtain a certain roll angle within a certain amount of time. It consists of three components; a linear model, a parameter estimation method and a V_c prediction model. These VPS components were designed for a simulation model of the Piper Seneca. This study analyzes the sensitivity of the VPS design to a change in aircraft dynamics and simulation model complexity by redesigning this system for a high-fidelity simulation model of the Fokker 50. The results show that both aircraft favor a small linear model and the Modified Kalman Method for parameter estimation. The original V_c prediction model however gives higher V_c prediction errors for the Fokker 50 than for the Piper Seneca. By simplifying the original V_c prediction model a stable, smooth and relatively accurate V_c prediction for the Fokker 50 can be obtained.

Nomenclature

Abbreviations

AFM	Aircraft Flight Manual
FA	Forgetting Algorithm
FAD	Forgetting Algorithm with Damping
FAR	Federal Aviation Regulations
JAR	Joint Aviation Requirements
LOC-I	Loss of Control In-flight
MKM	Modified Kalman Method
OEI	One-engine-inoperative
OLS	Ordinary Least Squares
PRESS	Prediction Sum of Squares
RLS	Recursive Least Squares
SD	Standard Deviation
SRS	Simona Research Simulator
SSE	Sum of Squared Errors
VPS	V_c Prediction System

Symbols

α	Real part of a complex number
β	Sideslip angle, Imaginary part of a complex number
δ	Deflection
ϕ	Roll angle
ϕ_{req}	Required roll angle
ρ	Air density
a	Aileron, Acceleration

b	Wing span
C	Coefficient, Correction
c	Constant
D	Discriminant
f	Flap
G	Gearing
L	Left
l	Rolling moment
m	Mass
n	Yawing moment
P	Constant
p	Roll rate
Q	Constant
q	Pitch rate
R	Right, Constant
r	Rudder, Yaw rate, Constant
S	Wing area, Constant
T	Thrust, Tail, Time period
t	Time
TO	Tail off
V	Velocity
V_0	Current air speed
V_c	Minimum lateral control speed
V_{c_L}	Minimum lateral control speed for a left roll
V_{c_R}	Minimum lateral control speed for a right roll
V_{mca}	Minimum control speed air
V_{TAS}	True air speed
x	x-direction in the body axes
Y	Sideforce
y	y-direction in the body axes
z	z-direction in the body axes

1 Introduction

Loss of Control In-flight (LOC-I) is one of the major causes of fatal accidents in commercial aviation.[1] It occurs when an aircraft uncontrollably deviates from its intended flight path, which usually follows from a complex chain of events such as structural or mechanical failures, loss of airspeed or combinations of these causes. Due to the variety and complexity of these causes, finding a universal solution for preventing LOC-I is difficult. Most of the proposed solutions in the research area of preventing LOC-I therefore focus on a particular subset of LOC-I. Lateral LOC-I is an example of such a subset. It typically occurs after an asymmetric aircraft failure, such as a single-engine failure in a multi-engine aircraft, wing damage or loss of aileron or rudder control. One of the proposed solutions for preventing lateral LOC-I was published by Koolstra in 2017, which aims to aid pilots in manual recovery from roll-limited situations.[2] Koolstra argued that, after an asymmetric aircraft failure, pilots need an indicator of the lateral-directional control limits. Currently the only lateral-directional control limit used by pilots is the minimum control speed air (V_{mca}). It is defined in the US Electronic Code of Federal Regulations Title 14 §25.149 as the minimum velocity at which straight flight can be maintained with a maximum roll angle of 5 degrees, when the critical engine is inoperative and the non-critical engine operates at full power.[3] The problem with preventing lateral LOC-I using V_{mca} is that V_{mca} only applies after an engine failure in a multi-engine aircraft. It does not incorporate other asymmetric failures. Additionally, V_{mca} does not provide an indication of the aircraft's manoeuvrability, as it is determined for a static equilibrium condition. To solve this problem Koolstra designed a system, named the V_c Prediction System (VPS), that continually predicts the minimum lateral control speed V_c of an aircraft based on the estimated roll performance. It consists of three components; a linear model which models the aircraft's lateral dynamics, a parameter estimation method which estimates the parameters of the linear model online and a V_c prediction model which uses the estimated parameters to predict V_c. Koolstra carefully designed the linear model, the parameter estimation method and the V_c prediction model based on simulations that were done using a low-fidelity simulation model of the Piper Seneca.[2] The suitability of Koolstra's VPS design for other aircraft and more complex simulation models is currently unknown.

The aim of this study is to analyze how sensitive the Piper Seneca VPS design is to a change in aircraft dynamics and simulation model complexity. This is achieved by repeating

Koolstra's VPS design process with a simulation model of the Fokker 50 and comparing the resulting Fokker 50 VPS design to the Piper Seneca VPS design. The main difference between these aircraft is that the Piper Seneca is a light aircraft mainly used in general aviation, whereas the Fokker 50 is a mid-size passenger aircraft mainly used in commercial aviation. Furthermore, the Fokker 50 simulation model used for this study has a higher fidelity than the Piper Seneca simulation model used in Koolstra's research [2], as it is based on and validated with extensive flight test data. It is therefore interesting to investigate if the Fokker 50 VPS can use the same linear model, parameter estimation method and V_c prediction model as the Piper Seneca VPS to provide an accurate prediction of V_c. The VPS is redesigned for the Fokker 50 by selecting the optimal combination of linear model and parameter estimation method, and by evaluating the accuracy of the V_c prediction model based on 48 different failure simulations using the Fokker 50 simulation model. This study focuses on the sensitivity of these three VPS components only, which means that aircraft state estimation and presenting the predicted V_c to the pilots is beyond the scope.

This paper consists of seven sections. In Section 2 the differences in aircraft states and control inputs between the Piper Seneca and the Fokker 50 in a roll-limited simulation model are identified. Following a short description of Koolstra's VPS design in Section 3, the VPS is redesigned for the Fokker 50 in Section 4 by reselecting the linear model and the parameter estimation method, and calculating its V_c prediction error for various combinations of linear model and parameter estimation method using Koolstra's V_c prediction model. These resulting V_c prediction errors for the Fokker 50 are relatively large compared to the V_c prediction errors of the Piper Seneca. Therefore a simplified V_c prediction model is derived in Section 5. Section 6 discusses the results of the redesigned VPS. Based on the differences between the Piper Seneca VPS design and the Fokker 50 VPS design, Section 7 concludes on how sensitive the VPS design is to a change in aircraft dynamics and simulation model complexity.

2 Minimum control speed air

The starting point of the VPS sensitivity analysis is to identify the differences in aircraft states and control inputs between the Piper Seneca and the Fokker 50 in a roll-limited equilibrium situation. These differences are used to predict how the change in aircraft dynamics affects the Fokker 50 VPS redesign in Section 4. For this study the most interesting roll-limited situation is a single-engine failure, because Koolstra designed the VPS to replace V_{mca}. Therefore the states and control inputs of the Piper Seneca and the Fokker 50 are determined for straight flight, with the critical engine inoperative and the propeller feathered and the non-critical engine at full throttle. This is done by solving the three lateral non-dimensional equations of motion numerically for sideforce, rolling moment and yawing moment, in which the four independent variables are roll angle, sideslip angle, aileron deflection and rudder deflection. To solve three equations for four unknowns, one variable needs to be fixed to a constant value. The flight scenario determines which variable is fixed. After a single-engine failure in a twin-turboprop aircraft two scenarios can occur. In the first scenario the pilot maintains a zero sideslip angle for drag minimization, which means that the sideslip angle is fixed at zero. In the second scenario the aircraft is flying so slow that the pilot has to give full rudder input to maintain a constant heading, which means that the rudder is fixed at its maximum deflection. Koolstra determined the states and control inputs of the Piper Seneca in the full rudder deflection scenario, with the left engine at full throttle and the right engine inoperative and the propeller feathered. His most relevant results are summarized and elaborated upon in Section 2.1. Similarly, the states and control inputs of the Fokker 50 for the full rudder deflection scenario are determined in Section 2.2.

2.1 Piper Seneca states and control inputs

Koolstra determined the states and control inputs of the Piper Seneca after a single-engine failure numerically by solving the three lateral non-dimensional equations of motion for the sideslip angle, aileron deflection and roll angle, assuming straight and level flight with full rudder deflection.[2] As the Piper Seneca has counter-rotating propellers, it does not have a critical engine. The right engine was therefore randomly selected as the inoperative engine and the left engine was set to full throttle. The results are plotted in Figure 1.[2] It highlights various points of interest; point 1 where the sideslip angle is zero for drag minimization, point 2 where maximum aileron deflection is reached, point 3 where the fin stalls, point 4 where the roll angle is zero for passenger comfort and point 5 where the roll angle decreases below -5 degrees, which is defined as V_{mca}. It is observed that the slopes of the required sideslip and roll angles and the required aileron deflection at V_{mca} are steep. At the velocity of V_{mca}, the slopes of the required sideslip

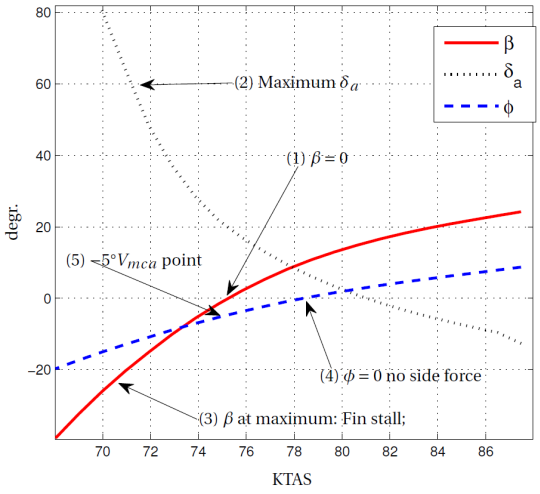

Figure 1: Numerically determined sideslip angle, aileron deflection and roll angle of the Piper Seneca as a function of air speed during straight and level flight with the left engine at full throttle, the right engine inoperative and the propeller feathered and full rudder deflection.[2]

angle, roll angle and aileron deflection are 4.0, 1.7 and -5.3 degrees per knot respectively. This indicates that lateral LOC-I in the Piper Seneca occurs rapidly with respect to air speed once V_{mca} is reached.

2.2 Fokker 50 states and control inputs

Similarly, the states and control inputs of the Fokker 50 after a single-engine failure are determined numerically for the full rudder deflection scenario by solving the three lateral non-dimensional equations of motion over a velocity range with full rudder deflection. This approach is similar to Koolstra's approach, but with a different model to fit the dynamics of the Fokker 50, different lateral aerodynamic and control coefficients and different engine data. The three lateral non-dimensional equations of motion are derived in Section 4-2-1 of [4], labeled as Equation 4-28. These equations are adjusted to represent steady straight flight and to account for asymmetric thrust. Terms which contain rotational rates, rotational accelerations and linear accelerations are therefore assumed to be zero, and thrust terms for each engine are added. The resulting equilibria in sideforce, rolling moment and yawing moment, denoted by subscripts Y, l and n are reflected by Equations 1, 2 and 3. In these equations the variables are roll angle ϕ, sideslip angle β, left and right aileron deflections δ_{a_L} and δ_{a_R}, rudder deflection δ_r and left and right thrust coefficients C_{T_L} and C_{T_R}. Each of these variables has a corresponding aerodynamic or control coefficient. Their values are determined from the data tables documented in [5], which have been generated from wind tunnel experiments and flight test data. These data tables are linearized around zero to obtain constant coefficients. Furthermore, the equations contain forces and moments caused by the thrust forces of the left and right engines and propellers T_L and T_R to account for asymmetric thrust. They are not non-dimensionalized like the other terms, because the required engine coefficients are not available from Fokker documentation. Instead, the engine forces and moments are identified from the Fokker 50 simulation model at two engine settings; inoperative with the propellers feathered and at full throttle. They are then modeled as a function of air speed and inserted into Equations 1, 2 and 3. Please note that the engine forces and moments are not the same as the coefficients related to the thrust coefficients C_{T_L} and C_{T_R}. These coefficients account for the propeller slipstream effects on the fuselage and tail, while the engine forces and moments account for the direct thrust of the propeller and jet stream, and the drag of the engine inlet.

$$\begin{aligned}\frac{mg}{\frac{1}{2}\rho V^2 S}\cdot\phi + &\left(C_{Y_{\beta_{TO}}} + C_{Y_{\beta_T}}\right)\cdot\beta + C_{Y_{\delta_{a_L}}}\delta_{a_L} + \\ &C_{Y_{\delta_{a_R}}}\delta_{a_R} + C_{Y_{\delta_r}}\delta_r + C_{Y_{C_{T_L}}}C_{T_L} + \\ &C_{Y_{C_{T_R}}}C_{T_R} + \frac{Y_{T_L}}{\frac{1}{2}\rho V^2 S} + \frac{Y_{T_R}}{\frac{1}{2}\rho V^2 S} = 0\end{aligned} \tag{1}$$

$$\begin{aligned}0 + &\left(C_{l_{\beta_{TO}}} + C_{l_{\beta_T}}\right)\cdot\beta + C_{l_{\delta_{a_L}}}\delta_{a_L} + \\ &C_{l_{\delta_{a_R}}}\delta_{a_R} + C_{l_{\delta_r}}\delta_r + C_{l_{C_{T_L}}}C_{T_L} + \\ &C_{l_{C_{T_R}}}C_{T_R} + \frac{l_{T_L}}{\frac{1}{2}\rho V^2 S b} + \frac{l_{T_R}}{\frac{1}{2}\rho V^2 S b} = 0\end{aligned} \tag{2}$$

$$\begin{aligned}0 + &\left(C_{n_{\beta_{TO}}} + C_{n_{\beta_T}}\right)\cdot\beta + C_{n_{\delta_{a_L}}}\delta_{a_L} + \\ &C_{n_{\delta_{a_R}}}\delta_{a_R} + C_{n_{\delta_r}}\delta_r + C_{n_{C_{T_L}}}C_{T_L} + \\ &C_{n_{C_{T_R}}}C_{T_R} + \frac{n_{T_L}}{\frac{1}{2}\rho V^2 S b} + \frac{n_{T_R}}{\frac{1}{2}\rho V^2 S b} = 0\end{aligned} \tag{3}$$

The left and right aileron deflections δ_{a_L} and δ_{a_R} are modeled separately such that their corresponding control coefficients can be taken directly from [5]. Since this leads to an extra independent variable, an extra equation is needed to solve the three lateral non-dimensional equations of motion. Equation 4 relates the left aileron deflection to the right aileron deflection by the gearing G. In reality this gearing varies along the entire deflection range of the ailerons.

However, to keep the model quasi-linear, it is assumed to be constant in each direction of deflection. Its value depends on the sign of the deflection to ensure that a maximum upward deflection of -33 degrees of the left aileron equals a maximum downward deflection of 22 degrees of the right aileron and vice versa.

$$\delta_{a_L} - G \cdot \delta_{a_R} = 0 \quad \text{with} \quad G = \frac{22}{-33} \quad \text{when} \quad \delta_{a_L} >= 0 \quad (4)$$
$$G = \frac{-33}{22} \quad \text{when} \quad \delta_{a_L} < 0$$

Geometric and mass properties of the Fokker 50 which are required to solve the three lateral non-dimensional equations of motion are listed in Table 1. Furthermore, the gear and flaps are fully retracted.

Property	Symbol	Value	Unit
Mass	m	17000	kg
Wing area	S	70	m^2
Wing span	b	29	m

Table 1: Fokker 50 properties used in the three lateral non-dimensional equations of motion for the numerical determination of the states and control inputs after a single-engine failure.

Using these data, the three lateral non-dimensional equations of motion are solved for the Fokker 50 with a full rudder deflection of -20 degrees. The left engine is inoperative and the propeller is feathered, and the right engine is set to full throttle, because the left engine is the critical engine of the Fokker 50. The results are shown in Figure 2. Comparing this figure to Figure 1 shows three differences. First, the plot is mirrored around the x-axis, because for the Fokker 50 the left engine is inoperative instead of the right engine. Second, point 3 which indicates fin stall is not indicated, because the drag of the vertical tail increases the yawing moment generated by the vertical tail when the sideslip angle increases even after the fin stalls, as shown in Figure 7.2.3b of [5]. Third, the slopes of the required roll and sideslip angles at V_{mca} for the Fokker 50 are a factor 10 smaller than for the Piper Seneca, with values of -0.5 and -0.2 degrees per knot respectively. This means that lateral LOC-I due to a single-engine failure occurs more gradually in the Fokker 50 than in the Piper Seneca when the air speed decreases. More importantly, the slope of the total aileron deflection at V_{mca} is only 0.8 degrees per knot, compared to -5.3 degrees per knot for the Piper Seneca. Since the V_c prediction model predicts the velocity at which a certain roll performance can be achieved based on the estimated available aileron deflection, this could lead to larger V_c prediction errors for the Fokker 50.

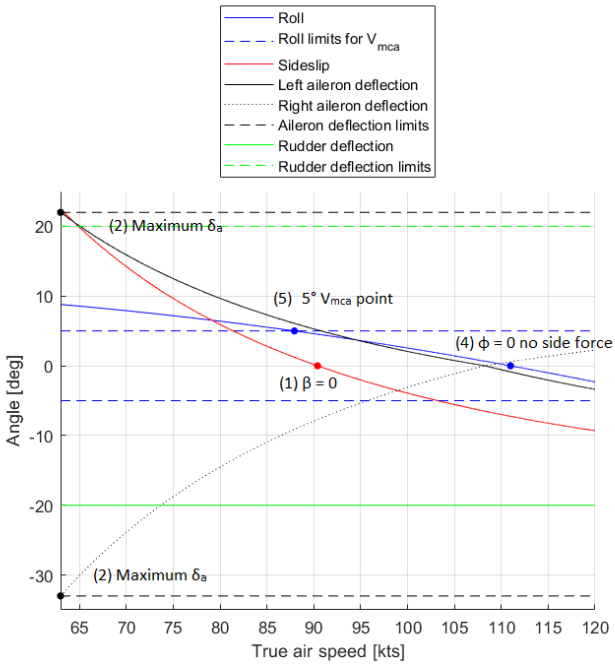

Figure 2: Numerically determined roll angle, sideslip angle and control surface deflections of the Fokker 50 as a function of air speed during straight and level flight with the left engine inoperative and the propeller feathered, the right engine at full throttle and full rudder deflection.

3 Description of the VPS

A short description of Koolstra's Piper Seneca VPS design is given to gain a better understanding of how it was designed and how it works. The VPS predicts the velocity V_c at which the aircraft can obtain a certain roll angle within a certain amount of time during a maximum performance roll to the left or to the right.[2] It uses three lateral equations of motion to capture the aircraft's roll dynamics in the linear model described in Section 3.1. The parameters of this linear model are estimated online by one of four parameter estimation methods listed in Section 3.2. The estimated parameters are then used by the V_c prediction model described in Section 3.3 to predict V_c. The three sections below do not

only describe these three VPS components in detail, they also explain which options were considered by Koolstra for the design of the Piper Seneca VPS. Please refer to Chapters 4, 5 and 6 of [2] for the full derivation and design of the Piper Seneca VPS.

3.1 Linear model

The linear model was derived by Koolstra to model the aircraft's lateral dynamics during a maximum performance roll.[2]. It consists of three lateral equations of motion around an arbitrary reference point to account for an unknown location of the center of gravity due to a structural failure. They were derived from Newton's second law, using a first order Taylor expansion to model the external forces. The entire linear model, which calculates the sideslip angle derivative $\dot{\beta}$, the roll angular acceleration $\dot{p}$ and the yaw angular acceleration $\dot{r}$ is stated below in Equations 5, 6 and 7 respectively. It should be noted that the terms T_L and T_R represent the torque percentages generated by the engines over the third power of the true air speed. This third power is required to obtain constant model parameters for an aircraft with turboprop engines.[2]

$$\begin{aligned}\frac{b\dot{\beta}}{V} =& Y_\beta\beta + Y_\phi\phi + Y_p\cdot\frac{pb}{2V} + Y_r\cdot\frac{rb}{2V} + Y_{\delta_a}\delta_a + \\ & Y_{\delta_r}\delta_r + Y_{T_L}T_L + Y_{T_R}T_R + Y_{a_z}\frac{a_z b}{2V^2} + Y_{\delta_f}\delta_f + \\ & Y_x\left(\frac{pb}{2V}\frac{rb}{2V} - 0.5\frac{\dot{r}b^2}{2V^2}\right) + \\ & Y_y\left(\left(\frac{pb}{2V}\right)^2 + \left(\frac{rb}{2V}\right)^2\right) + \\ & Y_z\left(\frac{qb}{2V}\frac{rb}{2V} - 0.5\frac{\dot{p}b^2}{2V^2}\right) + Y_{{\delta_a}^3}{\delta_a}^3 + Y_{\beta^2}\beta^2\end{aligned} \tag{5}$$

$$\begin{aligned}\frac{b^2\dot{p}}{2V^2} =& l_\beta\beta + l_\phi\phi + l_p\cdot\frac{pb}{2V} + l_r\cdot\frac{rb}{2V} + l_{\delta_a}\delta_a + \\ & l_{\delta_r}\delta_r + l_{T_L}T_L + l_{T_R}T_R + l_{a_z}\frac{a_z b}{2V^2} + l_{\delta_f}\delta_f + \\ & l_{\dot{q}}\frac{\dot{q}b^2}{2V^2} + l_{pq}\frac{pb}{2V}\frac{qb}{2V} + l_{qr}\frac{qb}{2V}\frac{rb}{2V} + \\ & l_{pr}\frac{pb}{2V}\frac{rb}{2V} + l_{q^2}\left(\frac{qb}{2V}\right)^2 + l_{r^2}\left(\frac{rb}{2V}\right)^2 + \\ & l_{p^2}\left(\frac{pb}{2V}\right)^2 + l_{a_x}\frac{a_x b}{2V^2} + l_{a_y}\frac{a_y b}{2V^2} + l_{{\delta_a}^3}{\delta_a}^3 + \\ & l_{\beta^2}\beta^2\end{aligned} \tag{6}$$

$$\begin{aligned}\frac{b^2\dot{r}}{2V^2} =& n_\beta\beta + n_\phi\phi + n_p\cdot\frac{pb}{2V} + n_r\cdot\frac{rb}{2V} + n_{\delta_a}\delta_a + \\ & n_{\delta_r}\delta_r + n_{T_L}T_L + n_{T_R}T_R + n_{a_z}\frac{a_z b}{2V^2} + n_{\delta_f}\delta_f + \\ & n_{\dot{q}}\frac{\dot{q}b^2}{2V^2} + n_{pq}\frac{pb}{2V}\frac{qb}{2V} + n_{qr}\frac{qb}{2V}\frac{rb}{2V} + \\ & n_{pr}\frac{pb}{2V}\frac{rb}{2V} + n_{q^2}\left(\frac{qb}{2V}\right)^2 + n_{r^2}\left(\frac{rb}{2V}\right)^2 + \\ & n_{p^2}\left(\frac{pb}{2V}\right)^2 + n_{a_x}\frac{a_x b}{2V^2} + n_{a_y}\frac{a_y b}{2V^2} + n_{{\delta_a}^3}{\delta_a}^3 + \\ & n_{\beta^2}\beta^2\end{aligned} \tag{7}$$

After this linear model was derived, Koolstra's main goal was to select the terms which resulted in the highest prediction accuracy of a maximum performance roll. Together these selected terms would form the optimal model for the Piper Seneca VPS. To prepare for the term selection process, the entire linear model was split up into a basic model containing 10 terms and 14 remaining additional terms. The 10 terms of the basic model are listed in Table 2a. Table 2b lists the 14 additional terms.

3.2 Parameter estimation method

The parameters of the linear model are estimated by a parameter estimation method. Since the VPS requires the parameters to be estimated online, the parameter estimation method needs to be recursive. Koolstra considered four parameter estimation methods for the Piper Seneca VPS: Recursive Least Squares (RLS) [6], a Forgetting Algorithm with Damping (FAD) with $\lambda = 0.995$ and $\delta = 200$ [7], the Modified Kalman Method (MKM) [6] and a Forgetting Algorithm (FA) with $\lambda = 0.9975$ [8][9]. Koolstra selected one of these four parameter estimation methods by combining them with three linear model sizes and calculating the means and standard deviations of the V_c prediction errors of each combination. Based on these values, it was concluded that the combination of the basic linear model and the MKM formed the optimal configuration of the Piper Seneca VPS.

3.3 V_c prediction model

The V_c prediction model predicts at which velocity V_c the aircraft can obtain the required roll angle ϕ_{req} within the time period T using the estimated linear model parameters. To obtain a V_c prediction from these inputs Koolstra derived a model which predicts the roll angle ϕ as a function of time t during a maximum performance roll to the left and to the

ID	Term	Parameter		
		Sideslip	Roll	Yaw
B1	β	Y_β	l_β	n_β
B2	ϕ	Y_ϕ	l_ϕ	n_ϕ
B3	$\frac{pb}{2V}$	Y_p	l_p	n_p
B4	$\frac{rb}{2V}$	Y_r	l_r	n_r
B5	δ_a	Y_{δ_a}	l_{δ_a}	n_{δ_a}
B6	δ_r	Y_{δ_r}	l_{δ_r}	n_{δ_r}
B7	T_L	Y_{T_L}	l_{T_L}	n_{T_L}
B8	T_R	Y_{T_R}	l_{T_R}	n_{T_R}
B9	$\frac{a_z b}{2V^2}$	Y_{a_z}	l_{a_z}	n_{a_z}
B10	δ_f	Y_{δ_f}	l_{δ_f}	n_{δ_f}

(a) Basic linear model terms.[2]

ID	Term	Parameter		
		Sideslip	Roll	Yaw
1	$\frac{pb}{2V}\frac{rb}{2V} - 0.5\frac{\dot{r}b^2}{2V^2}$	Y_x	-	-
2	$(\frac{pb}{2V})^2 + (\frac{rb}{2V})^2$	Y_y	-	-
3	$\frac{qb}{2V}\frac{rb}{2V} - 0.5\frac{\dot{p}b^2}{2V^2}$	Y_z	-	-
4	$\frac{\dot{q}b^2}{2V^2}$	-	$l_{\dot{q}}$	$n_{\dot{q}}$
5	$\frac{pb}{2V}\frac{qb}{2V}$	-	l_{pq}	n_{pq}
6	$\frac{qb}{2V}\frac{rb}{2V}$	-	l_{qr}	n_{qr}
7	$\frac{pb}{2V}\frac{rb}{2V}$	-	l_{pr}	n_{pr}
8	$(\frac{qb}{2V})^2$	-	l_{q^2}	n_{q^2}
9	$(\frac{rb}{2V})^2$	-	l_{r^2}	n_{r^2}
10	$(\frac{pb}{2V})^2$	-	l_{p^2}	n_{p^2}
11	$\frac{ba_x}{2V^2}$	-	l_{a_x}	n_{a_x}
12	$\frac{ba_y}{2V^2}$	-	l_{a_y}	n_{a_y}
13	${\delta_a}^3$	$Y_{{\delta_a}^3}$	$l_{{\delta_a}^3}$	$n_{{\delta_a}^3}$
14	β^2	Y_{β^2}	l_{β^2}	n_{β^2}

(b) Additional linear model terms.[2]

Table 2: List of the linear model terms, including term identifiers and the corresponding model parameters.[2]

right.[2] The starting point of the derivation is Equation 6. All but the roll rate and the aileron terms are temporarily discarded from the right-hand side of this equation, under the assumptions that the sideslip angle and the yaw rate are zero, and that the load factor and the engine settings are constant. This results in the first order linear differential equation shown in Equation 8. To account for the discarded model terms, the aileron deflection δ_a is changed to the total available aileron deflection $\delta_{a_{av}}$, which is the available aileron travel for the maximum performance roll.

$$\frac{b^2\dot{p}}{2V^2} = l_p \cdot \frac{pb}{2V} + l_{\delta_a}\delta_{a_{av}} \tag{8}$$

After solving this differential equation for the roll rate as function of time using $p(0) = 0$ radians per second as an initial condition, integrating once more using $\phi(0) = \phi_0$ radians as an initial condition, and substituting $\phi(\mathrm{T}) = \phi_{req} + \phi_0$, the total available aileron deflection $\delta_{a_{av}}$ is calculated and substituted. This total available aileron deflection $\delta_{a_{av}}$ is defined as the difference between the aileron limits, the current aileron deflection $\delta_{a_{V_0}}$ and 9 corrections denoted by C in Table 3. For the definitions and equations of these corrections please refer to [2].

Correction	Description
C_1	Roll constant at $V = 0$
C_2	Change of roll constant with V_{TAS}
C_3	Current $\dot{p}$ and p
C_4	Thrust asymmetry
C_5	Maximum δ_r
C_6	Asymmetric mass
C_9	Roll coupling
C_{10}	Maximum δ_r in OEI
C_{11}	Adverse yaw

Table 3: Corrections for the total available aileron deflection $\delta_{a_{av}}$ used in the V_c prediction model.[2]

Finally the total available aileron deflection for a maximum performance left and right roll is predicted with Equations 9 and 10 respectively. The independent variables in these equations are the predicted V_c for a left roll V_{c_L} and the predicted V_c for a right roll V_{c_R}. If valid solutions for V_{c_L} and V_{c_R} exist, a damped and limited Newton's method is used to determine V_{c_L} and V_{c_R}. This damped and limited Newton's method uses the predicted V_c from the previous time step as a starting point, and does only one iteration per time step with a maximum velocity step of 0.5 meters per second. This is different from the regular Newton's method, which keeps iterating until the solution has converged to a certain velocity error. In addition to limiting and damping Newton's method, the resulting values of V_{c_L} and V_{c_R} are clipped between 25 meters per second and the current velocity $V_0 + 15$ meters per second to remove peaks from the predicted V_c. If no valid solution to Equations 9 or 10 exists, V_{c_L} or V_{c_R} is set to 25 meters per second. Finally the output of the V_c prediction model, which is the predicted V_c, is found by taking the maximum value of V_{c_L} and V_{c_R}.

$$
\begin{aligned}
0 = &- \phi_{req_L} + \left(C_1 \cdot V_{c_L} + C_2 \cdot V_{c_L}^2\right) \cdot \\
&\left(\frac{-2 \cdot l_{\delta_a}}{b \cdot l_p}\right) \cdot \Bigg[\delta_{a_{max}} - \delta_{a_{V_0}} + C_3 \\
&- C_4 \cdot \left(\frac{V_0^2}{V_{c_L}^2} - 1\right) - C_6 \cdot \left(\frac{V_0^2}{V_{c_L}^2} - 1\right) \\
&- C_{5_L} - C_{9_L} - C_{10_L} - C_{11_L}\Bigg]
\end{aligned} \tag{9}
$$

$$
\begin{aligned}
0 = &- \phi_{req_R} + \left(C_1 \cdot V_{c_R} + C_2 \cdot V_{c_R}^2\right) \cdot \\
&\left(\frac{-2 \cdot l_{\delta_a}}{b \cdot l_p}\right) \cdot \Bigg[\delta_{a_{min}} - \delta_{a_{V_0}} + C_3 \\
&- C_4 \cdot \left(\frac{V_0^2}{V_{c_R}^2} - 1\right) - C_6 \cdot \left(\frac{V_0^2}{V_{c_R}^2} - 1\right) \\
&- C_{5_R} - C_{9_R} - C_{10_R} - C_{11_R}\Bigg]
\end{aligned} \tag{10}
$$

The exact same V_c prediction model is used for the redesign of the Fokker 50 VPS in Section 4, except for the inputs ϕ_{req} and T. The Piper Seneca VPS used a required roll angle of $\phi_{req} = 30$ degrees within a time period of $T = 1.5$ seconds. Table XXVIII in Mil. Spec. 1797 prescribes that the Fokker 50, a class II-L aircraft, in category C conditions requires $\phi_{req} = 30$ degrees of roll in $T = 1.8$ seconds or less for level 1 handling qualities.[10] These values are therefore used as inputs for Koolstra's V_c prediction model instead.

4 Fokker 50 VPS redesign

The VPS is redesigned for the Fokker 50 by repeating Koolstra's VPS design process described in Chapters 5 and 6 of [2]. The design process consists of three steps. First, in Section 4.1 Koolstra's 48 hypothetical failure simulations, on which the Fokker 50 VPS design choices are based, are simulated using the Fokker 50 simulation model. Second, in Section 4.2 additional terms of the linear model described in Section 3.1 are selected, which leads to three suggested linear models. Third, in Section 4.3 these three linear models are combined with the four parameter estimation methods listed in Section 3.2, to determine which combination gives the lowest V_c prediction error with Koolstra's V_c prediction model.

4.1 Failure simulations

The first step in redesigning the VPS for the Fokker 50 is to generate data on which linear model term selection and parameter estimation method selection is based. Koolstra performed 48 different simulations with the Piper Seneca simulation model controlled by an autopilot. During these simulations the autopilot tracked altitude and velocity reference trajectories for 170 seconds. After that, the aircraft performed a maximum performance roll. Four different variations were added to the simulations by introducing the failures listed in Table 4, switching turbulence on or off, giving one or two sinusoidal input signals on the control surfaces to excite the system and by performing the maximum performance roll to the left or right.

Failure	**Roll direction**	**Runs**
No failure	Left and right	8
50% loss of aileron	Left and right	8
100% loss of rudder	Left and right	8
Left engine failure	Right	4
Right engine failure	Left	4
Asymmetry left wing heavy	Right	4
Asymmetry right wing heavy	Left	4
Rudder hardover to the left	Right	4
Rudder hardover to the right	Left	4

Table 4: List of the failure types, roll direction during the maximum performance roll and the amount of simulations out of the total of 48 simulations.[2]

These 48 simulations are recreated with the Fokker 50 simulation model by tracking similar altitude and velocity reference signals using a custom-made autopilot. The four variations are replicated as well. First, the failures listed in Table 4 are activated after 30 seconds. 50% loss of aileron and 100% loss of rudder are simulated by fixing the right aileron and the rudder at zero degrees deflection. Rudder hardover is simulated by fixing the rudder at maximum deflection. Left wing and right wing mass asymmetries are simulated by shifting the center of gravity 0.25 meters to the left and right. Second, turbulence is generated using the Joint Aviation Regulations (JAR) turbulence generator that was included in the Fokker 50 simulation model. Third, input signals are applied after 30 and optionally 90 seconds to all primary lateral controls including the throttle levers as a single sine wave with an amplitude of 10 degrees and a period of 5 seconds. Fourth, the maximum performance rolls are simulated by applying an instant minimum or maximum

aileron deflection after 170 seconds. To provide an example of the trajectory of one of the 48 simulations, the velocity and altitude of a simulation with 50% loss of aileron, no turbulence, one set of control inputs and a left roll is plotted in Figures 3a and 3b. These figures are similar to Figures 5.2b and 5.2c presented in [2], which present the velocity and altitude of the Piper Seneca during the same simulation.

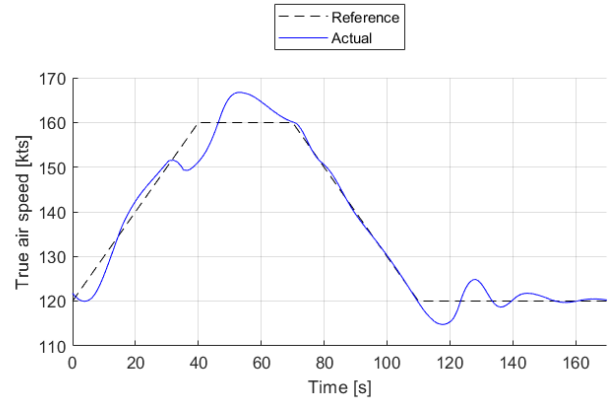

(a) Velocity.

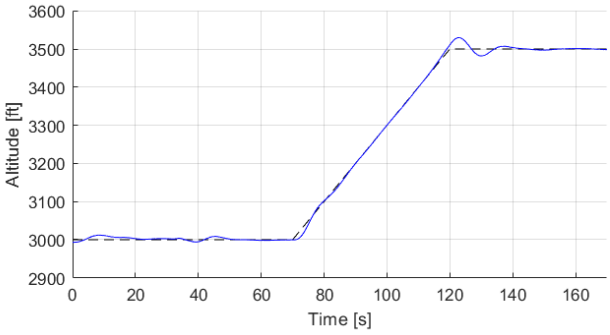

(b) Altitude.

Figure 3: Trajectory of the Fokker 50 during a simulation with 50% loss of aileron, no turbulence, one set of control inputs and a maximum performance roll to the left.

4.2 Linear model selection

The second step in redesigning the VPS for the Fokker 50 is to reselect the linear model based on the 48 failure simulations, which is done by repeating the selection process described in Chapter 5 of [2]. In the derivation of the V_c prediction model Koolstra obtained linear models for the sideslip angle derivative, the roll angular acceleration and the yaw angular acceleration. These three models contain a total of 24 different terms, which altogether form the **entire model**. To determine which of these terms are most capable of predicting the model outputs during the maximum performance rolls, Koolstra selected 10 terms to form a **basic model**. The 14 additional terms were either accepted or omitted through a selection process.

This selection process works a follows. The data from the simulations up to the maximum performance roll were used to estimate the parameters of the linear model offline using an Ordinary Least Squares (OLS) estimator. With these estimated parameters the three model outputs during the maximum performance roll were predicted. Each of these three model outputs were integrated once with the Runge Kutta method, to obtain predictions of the sideslip angle, the roll rate and the yaw rate during the maximum performance roll. The measured sideslip angle, roll rate and yaw rate at the start of the maximum performance roll were the initial conditions for this integration. Next, the accuracy of the predicted sideslip angle, roll rate and yaw rate was evaluated with one of six term selection methods, and the decision to accept or omit a term was made. Accepting or omitting additional model terms was a sequential process. Starting with the basic model, each additional model term was sequentially added to the current model and subjected to one of six selection methods. Based on the outcome, the additional term was either definitely added to the current linear model, or omitted. Therefore the order in which terms were added to the linear model affected the decision of accepting or omitting the remaining additional model terms. The intermediate result was a **final model** for each of the 48 simulations, which contained the additional terms that were accepted for that particular simulation. The desired end result was a single **optimal model**, which was obtained by composing a list of selection rates for each additional term over all 48 simulations and selecting three terms with relatively high selection rates to form the optimal model for the Piper Seneca. Finally this optimal model was evaluated based on its prediction errors.

This process is repeated to obtain similar results for the Fokker 50. The process starts by selecting the additional linear model terms using a one of Koolstra's six term selection methods in Section 4.2.1. Based on the resulting selection rates of the additional terms in the final models, an optimal model for the Fokker 50 is formed in Section 4.2.2. This optimal model is evaluated based on its prediction errors in Section 4.2.3.

4.2.1 Term selection method

The final models for each failure simulation of the Fokker 50 are found by choosing and applying one of the six selection methods used by Koolstra to the simulated data.[2] Initially Koolstra considered four different statistical selection methods, which all had a tendency to over-fit. These methods selected too many additional terms, which increased the prediction errors of the final models. Two 'Alternate methods' were therefore developed based on the Prediction Sum of Squares (PRESS) method, which uses one part of a data set to train the model and the other part to quantify the prediction accuracy by squaring and summing the prediction errors.[11] The two 'Alternate methods' do the same, using the first part of the data set to estimate the model parameters and the maximum performance roll to rate the increase in prediction accuracy based on five evaluation steps. In these five steps, each additional term is judged on three criteria. The first criterion is that the additional term must have a collinearity lower than 95% with other terms that have already been selected. The second criterion is that the improvement in the Sum of Squared Errors (SSE) of the predicted sideslip angle, roll rate or yaw rate must be higher than the prediction uncertainty originating from the uncertainty of the OLS parameter estimate. The third criterion is that the increased prediction accuracy must be significant, with a margin of at least one percent improvement of the SSE. The difference between the two 'Alternate methods' is that the regular 'Alternate method' selects terms based on the sideslip, roll and yaw equations, whereas the 'Alternate method - ϕ' selects terms based on the roll equation only. Koolstra decided to select the model terms with the regular 'Alternate method', because the 'Alternate method - ϕ' might give inaccurate predictions for sideslip and yawing motion. Therefore the regular 'Alternate method' is used to select the terms of the optimal model for the Fokker 50 as well.

4.2.2 Optimal model selection

Using Koolstra's regular 'Alternate method' as a selection method the selection rates of the additional terms in the final models are found, which finally leads to the optimal model containing the most relevant additional terms. The selection rates for the additional terms in the final models are shown in Table 5, along with the selection rates found by Koolstra for the additional terms of the Piper Seneca.[2] Two differences between the selection rates for Piper Seneca and the Fokker 50 are observed. First, the mean selection rate for additional terms of the yaw equation is more than

ID	Term	Selection rates [%]	
		Piper Seneca	**Fokker 50**
1	$\frac{pb}{2V}\frac{rb}{2V} - 0.5\frac{\dot{r}b^2}{2V^2}$	0.0	18.8
2	$(\frac{pb}{2V})^2 + (\frac{rb}{2V})^2$	**20.8**	33.3
3	$\frac{qb}{2V}\frac{rb}{2V} - 0.5\frac{\dot{p}b^2}{2V^2}$	0.0	43.8
13	${\delta_a}^3$	22.9	**39.6**
14	β^2	14.6	4.2
Mean		**11.7**	**27.9**

(a) Sideslip equation.

ID	Term	Selection rates [%]	
		Piper Seneca	**Fokker 50**
4	$\frac{\dot{q}b^2}{2V^2}$	0.0	10.4
5	$\frac{pb}{2V}\frac{qb}{2V}$	**12.5**	10.4
6	$\frac{qb}{2V}\frac{rb}{2V}$	0.0	2.1
7	$\frac{pb}{2V}\frac{rb}{2V}$	6.3	2.1
8	$(\frac{qb}{2V})^2$	2.1	8.3
9	$(\frac{rb}{2V})^2$	8.3	6.3
10	$(\frac{pb}{2V})^2$	**31.3**	18.8
11	$\frac{ba_x}{2V^2}$	4.2	6.3
12	$\frac{ba_y}{2V^2}$	4.2	2.1
13	${\delta_a}^3$	2.1	**47.9**
14	β^2	4.2	22.9
Mean		**6.8**	**12.5**

(b) Roll equation.

ID	Term	Selection rates [%]	
		Piper Seneca	**Fokker 50**
4	$\frac{\dot{q}b^2}{2V^2}$	10.4	0.0
5	$\frac{pb}{2V}\frac{qb}{2V}$	**37.5**	6.3
6	$\frac{qb}{2V}\frac{rb}{2V}$	22.9	6.3
7	$\frac{pb}{2V}\frac{rb}{2V}$	25.0	8.3
8	$(\frac{qb}{2V})^2$	14.6	6.3
9	$(\frac{rb}{2V})^2$	22.9	6.3
10	$(\frac{pb}{2V})^2$	**41.7**	12.5
11	$\frac{ba_x}{2V^2}$	0.0	4.2
12	$\frac{ba_y}{2V^2}$	8.3	2.1
13	${\delta_a}^3$	18.8	**22.9**
14	β^2	20.8	12.5
Mean		**20.3**	**8.0**

(c) Yaw equation.

Table 5: Selection rates for the additional model terms.

twice as small for the Fokker 50, which means that the additional yaw terms do not improve the yaw rate prediction for the Fokker 50 as much as for the Piper Seneca. The opposite is true for the sideslip and roll equations. Second, term 13, which is the term that represents non-linear aileron effects, is an important term for the roll equation of the Fokker 50. Since the output of VPS is based on the predicted roll performance, this term is included in the optimal model for the Fokker 50, whereas Koolstra selected terms 2, 5 and 10 for the optimal model of the Piper Seneca. In short, the optimal model for the Fokker 50 is a combination of the basic model and additional term 13.

4.2.3 Optimal model evaluation

The prediction errors of this newly found optimal model are compared to the prediction errors of the basic model, the final models and the entire model to evaluate the performance of the optimal model. These prediction errors are obtained by taking the mean SSE of the sideslip angle, roll rate and yaw rate over all 48 simulations. The results for the Piper Seneca in Table 6a show that the final models have a lower prediction error than the basic model, which means that the term selection process improved the overall prediction accuracy.[2] Also, the optimal model has a higher prediction error than the basic model, which was described by Koolstra as over-fitting. Similar results are obtained for the Fokker 50 in Table 6b. The final models have a lower prediction error than the basic model, while the optimal model shows mixed results.

Variable	**Unit**	**Model**		
		Basic	**Final**	**Optimal**
Sideslip angle	rad^2	0.4453	0.3494	1.0528
Roll rate	$(rad/s)^2$	0.0226	0.0160	0.0719
Yaw rate	$(rad/s)^2$	0.0127	0.0077	0.0211

(a) Piper Seneca.[2]

Variable	**Unit**	**Model**		
		Basic	**Final**	**Optimal**
Sideslip angle	rad^2	0.0334	0.0104	0.0166
Roll rate	$(rad/s)^2$	0.2497	0.1215	0.5014
Yaw rate	$(rad/s)^2$	0.1127	0.0591	0.2556

(b) Fokker 50.

Table 6: Sum of the squared prediction errors for the three model equations of the basic model, the final models and the optimal model for the Fokker 50.

To obtain a more visual representation of the prediction errors of the linear model, the model outputs during the maximum performance roll of one of the 48 simulations are plotted next to the measured values. The predicted sideslip angle, roll rate and yaw rate during the maximum performance roll of the simulation with mass asymmetry with a heavy right wing, no turbulence, one set of control inputs and a maximum performance roll to the left are plotted in Figure 4. This figure is comparable to Figure 5.7 in [2], which shows the predicted sideslip angle and roll rate during the same simulation. The figure shows that the basic and final models are able to predict the roll rate relatively accurately, the optimal model over-estimates the roll rate and the entire model even diverges. At this stage the basic model therefore seems to be the most suitable for predicting a maximum performance roll of the Fokker 50. Following Koolstra's VPS design process however, the basic model, the optimal model and the entire model are all considered for the selection of the optimal configuration of the Fokker 50 VPS in Section 4.3.

4.3 Parameter estimation method selection

The third step in redesigning the VPS for the Fokker 50 is to choose a configuration of linear model and parameter estimation method which gives the lowest V_c prediction error. Koolstra analyzed a total of 48 configurations for the VPS; three model sizes, four parameter estimation methods, two normalization options of the engine model and two initial velocities of 80 and 120 knots.[2] This study limits itself to 12 configurations; three linear model sizes and four parameter estimation methods. The normalization option is not considered, because it hardly affected the V_c prediction error of the VPS for the Piper Seneca. Furthermore, only the initial velocity of 120 knots is used, because the initial velocity of 80 knots is lower than the stall speed of the Fokker 50. The 12 combinations of linear model and parameter estimation method therefore consist of three linear models; the basic model, the optimal model and the entire model, and the four parameter estimation methods described in Section 3.2. These 12 configurations are all re-implemented in the Fokker 50 VPS, and they are used to calculate estimates of the linear model parameters online in each of the 48 simulations. With these estimated model parameters the V_c prediction model predicts V_c for each of the 12 configurations in each of the 48 simulations based on the maximum performance rolls. The final result is the mean and standard deviation of the V_c prediction error for each of the 12 configurations over the 48 simulations, from which

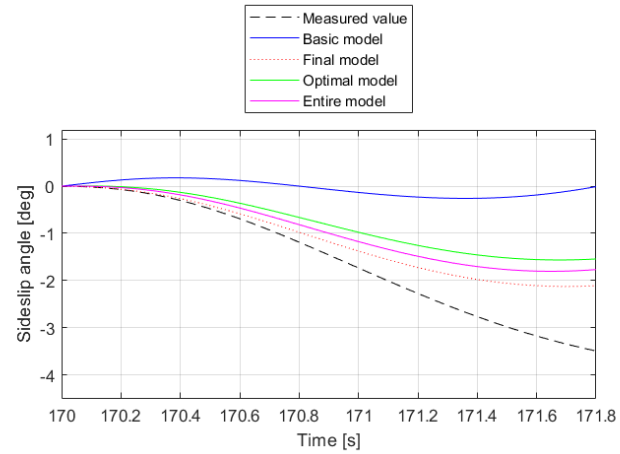

(a) Sideslip angle.

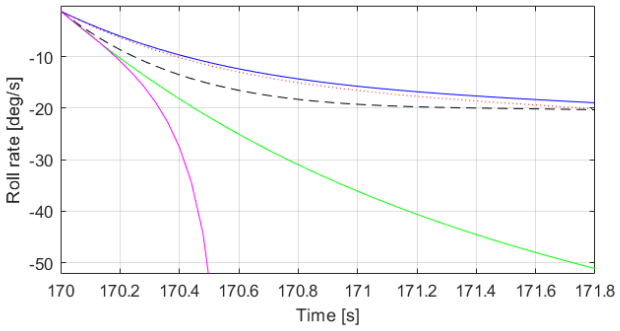

(b) Roll rate.

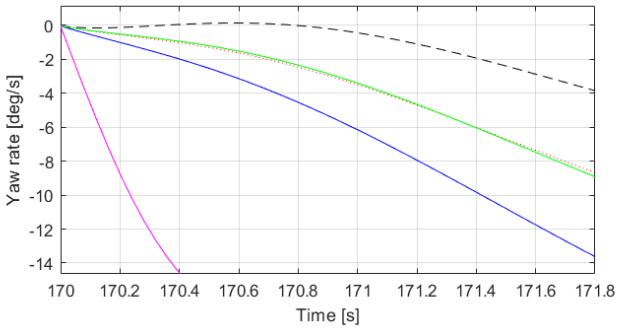

(c) Yaw rate.

Figure 4: Outputs of the linear models during a maximum performance roll with mass asymmetry with a heavy right wing, no turbulence, one set of control inputs and a maximum performance roll to the left.

the optimal VPS configuration is selected.

To calculate the V_c prediction error, the predicted V_c, which is the output of the VPS, needs to be compared with the actual V_c, which is the actual velocity at which the required roll angle of 30 degrees is reached within precisely 1.8 seconds during a maximum performance roll. The problem however, is that it would require a sequence of maximum performance rolls at a range of air speeds to the determine the actual V_c numerically. Koolstra found a solution by reversing the problem, using the measured change in roll angle achieved within the time period T during the maximum performance roll in each of the 48 simulations as input for the V_c prediction model, defining the resulting V_c as the predicted V_c, and defining the true air speed 0.5 seconds before the maximum performance roll as the actual V_c. Through this reversal, the predicted V_c can be compared directly to the actual V_c. This results in the mean and standard deviation of the V_c prediction error over each of the 48 simulations for each VPS configuration. Koolstra's results for the Piper Seneca in Table 7a show that four linear model and parameter estimation method combinations give a mean V_c prediction error of nearly 2.0 meters per second.[2] Koolstra decided to select the MKM and the basic linear model as the optimal configuration. The results for the Fokker 50 in Table 7b however show that the V_c prediction error is almost an order of magnitude larger for all configurations.

Model	**Size**		**RLS**	**FAD**	**MKM**	**FA**
Basic	10	Mean	2.1	3.0	**2.2**	2.8
		SD	2.3	3.3	**2.3**	2.7
Optimal	13	Mean	2.0	3.0	2.2	2.9
		SD	2.1	3.3	2.3	2.5
Entire	22	Mean	5.6	15.0	5.4	7.9
		SD	7.4	8.2	6.3	10.8

(a) Piper Seneca.[2]

Model	**Size**		**RLS**	**FAD**	**MKM**	**FA**
Basic	10	Mean	11.7	9.6	14.4	10.5
		SD	10.7	16.0	17.4	11.1
Optimal	11	Mean	12.7	26.3	15.6	13.3
		SD	11.4	17.4	17.6	16.2
Entire	24	Mean	12.6	31.2	18.4	13.1
		SD	10.6	11.6	21.0	16.2

(b) Fokker 50.

Table 7: Means and standard deviations of the V_c prediction errors for each VPS configuration in meters per second.

The cause of these disappointing results for the V_c prediction errors of the Fokker 50 is found by plotting the predicted V_c during the left engine failure simulation with one set of control inputs, turbulence on and the maximum performance roll to the right. Figure 5, which is comparable to Figure 6.9 in [2], plots the values of V_{c_L} and V_{c_R} as a function of time, as well as the true air speed using the basic model, the MKM and Koolstra's V_c prediction model. It clearly shows that the V_c prediction model struggles to find a stable solution. The V_c prediction model clips the V_c predictions to values between 25 and the true air speed plus 15 meters per second. Since Section 4.2.3 showed that the basic model accurately predicts the maximum performance roll, these large prediction errors must be caused by the V_c prediction model. Variations to Koolstra's V_c prediction model were therefore applied, such as setting all corrections and the current aileron deflection in Equations 9 and 10 to zero. This led to a mean prediction error of 5.2 meters per second with a standard deviation of 7.3 meters per second for the combination of basic model and MKM, hinting that Koolstra's V_c prediction model might be too complex for the Fokker 50 VPS. Therefore a new, simplified V_c prediction model was derived.

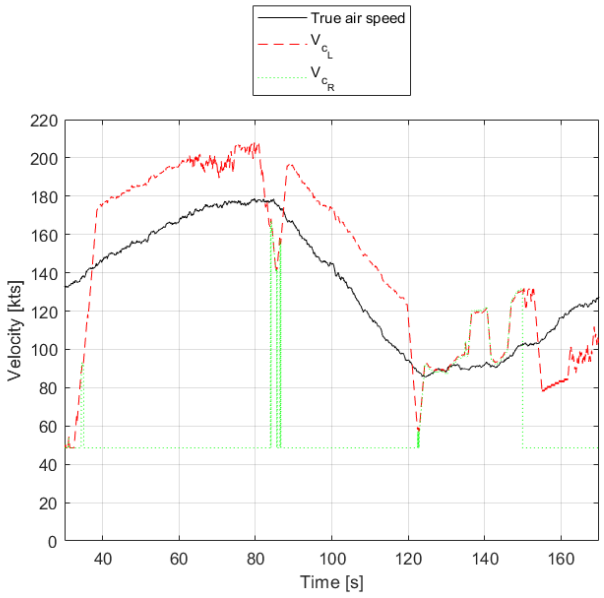

Figure 5: Predicted V_{c_L} and V_{c_R} during the left engine failure simulation with one set of control inputs, turbulence on and a maximum performance roll to the right using the basic model, the MKM and Koolstra's V_c prediction model.

5 Simplified V_c prediction model

A simplified V_c prediction model is derived to decrease the V_c prediction errors of the redesigned Fokker 50 VPS. The starting point of the derivation is the same as for Koolstra's V_c prediction model; Equation 6. Koolstra's approach to solving this equation was to substitute the total available aileron deflection $\delta_{a_{av}}$ for most of the right-hand terms, solving the resulting first order linear differential equation algebraically, and applying corrections for the available aileron travel later on. For simplification purposes however, this derivation solves Equation 6 directly for the roll angle ϕ as a function of time t without substituting $\delta_{a_{av}}$, such that no corrections are required. All aircraft states, control inputs and air path variables which are not derivatives of the roll angle are assumed to be constant during a maximum performance roll of 1.8 seconds. As a result, this equation can be re-written in the form of Equation 11 with the current roll angle and roll rate as initial conditions and the constants P, Q, R and S defined in Equations 12 to 15.

$$P\ddot{\phi}(t) + Q\dot{\phi}(t) + R\phi(t) = S \quad \text{with} \quad \begin{matrix}\phi(0) = \phi_0 \\ \dot{\phi}(0) = p_0\end{matrix} \tag{11}$$

$$P = \frac{b^2}{2V^2} \tag{12}$$

$$Q = -\frac{b}{2V} l_p \tag{13}$$

$$R = -l_\phi \tag{14}$$

$$S = l_\beta \beta + l_r \cdot \frac{rb}{2V} + l_{\delta_a}\delta_a + l_{\delta_r}\delta_r + l_{T_L}T_L + l_{T_R}T_R + l_{a_z}\frac{a_z b}{2V^2} + l_{\delta_f}\delta_f \tag{15}$$

This equation is a second order non-homogeneous linear differential equation with initial conditions $p(0)$=p_0 and $\phi(0)$=ϕ_0. It can have three different algebraic solutions, depending on the value of the discriminant D in Equation 16.[12].

$$D = Q^2 - 4PR \tag{16}$$

When $D > 0$ the roots of the auxiliary equation are real and distinct, which means that the general solution is given by Equation 17 with the constants defined in Equations 18 to 21. Substituting $\phi(T) = \phi_0 + \phi_{req}$ leads to Equation 22.

$$\phi(t) = c_1 e^{r_1 t} + c_2 e^{r_2 t} + \frac{S}{R} \tag{17}$$

$$r_1 = \frac{-Q - \sqrt{D}}{2P} \tag{18}$$

$$r_2 = \frac{-Q + \sqrt{D}}{2P} \tag{19}$$

$$c_2 = \frac{p_0 - r_1(\phi_0 - \frac{S}{R})}{r_2 - r_1} \tag{20}$$

$$c_1 = \phi_0 - \frac{S}{R} - c_2 \tag{21}$$

$$0 = -(\phi_0 + \phi_{req}) + c_1 e^{r_1 T} + c_2 e^{r_2 T} + \frac{S}{R} \tag{22}$$

When $D = 0$ the auxiliary equation has only one real root, which means that the general solution is given by Equation 23 with the constants defined in Equations 24 to 26. Substituting $\phi(T) = \phi_0 + \phi_{req}$ leads to Equation 27.

$$\phi(t) = c_1 e^{r_1 t} + c_2 t e^{r_1 t} + \frac{S}{R} \tag{23}$$

$$r_1 = \frac{-Q}{2P} \tag{24}$$

$$c_1 = \phi_0 - \frac{S}{R} \tag{25}$$

$$c_2 = p_0 - r_1 c_1 \tag{26}$$

$$0 = -(\phi_0 + \phi_{req}) + c_1 e^{r_1 T} + c_2 T e^{r_1 T} + \frac{S}{R} \tag{27}$$

When $D < 0$ the roots of the auxiliary equation ($\alpha - \beta i$ and $\alpha + \beta i$) lie in the complex plane, which means that the general solution is given by Equation 28 with the constants defined in Equations 29 to 32. Substituting $\phi(T) = \phi_0 + \phi_{req}$ leads to Equation 33.

$$\phi(t) = e^{\alpha t} \cdot [c_1 \cos(\beta t) + c_2 \sin(\beta t)] + \frac{S}{R} \tag{28}$$

$$\alpha = \frac{-Q}{2P} \tag{29}$$

$$\beta = \frac{\sqrt{-D}}{2P} \tag{30}$$

$$c_1 = \phi_0 - \frac{S}{R} \tag{31}$$

$$c_2 = \frac{p_0 - \alpha c_1}{\beta} \tag{32}$$

$$0 = -(\phi_0 + \phi_{req}) + e^{\alpha T} \cdot [c_1 \cos(\beta T) + c_2 \sin(\beta T)] + \frac{S}{R} \tag{33}$$

Depending on the value of the discriminant, Equation 22, 27 or 33 is solved for V_{c_L} and V_{c_R} with the bisection method. For a left roll ϕ_{req} is equal to -30 degrees and δ_a is equal to the minimum aileron deflection. For a right roll ϕ_{req} is equal to 30 degrees and δ_a is equal to the maximum aileron deflection. For all other aircraft states and control inputs the currently measured values are used. The bisection method has velocity bounds of 30 to 300 meters per second and a convergence error of 0.1 meters per second. The reason why the lower velocity bound is not 0 meters per second, is that these equations can have two solutions between 0 and 300 meters per second, the first of which usually lies between 0 and 30 meters per second. Additionally, these equations are undefined for $V = 0$. By using the bisection method instead of Newtons method, there is no need to calculate any function derivatives.

With this simplified V_c prediction model the mean V_c prediction errors are re-evaluated for the basic linear model and each of the four parameter estimation methods. The results in Table 8 show an improved V_c prediction accuracy for the MKM. The forgetting algorithms on the other hand perform worse. In an effort to improve their performance their forgetting factors are changed to 0.9 and 1.0. As a result, the mean V_c prediction error of the FAD changes to 193.5 and 22.9 meters per second respectively. The mean V_c prediction error of the FA is much less sensitive to these changes, with 100.5 and 95.8 meters per second respectively.

Model	**Size**		**RLS**	**FAD**	**MKM**	**FA**
Basic	10	Mean	15.8	152.7	**5.2**	95.8
		SD	14.0	92.3	**6.4**	82.8

Table 8: Means and standard deviations of the V_c prediction errors for each VPS configuration of the Fokker 50 in meters per second using the simplified V_c prediction model.

These results show that the optimal configuration for the Fokker 50 VPS is the basic model, the MKM and the simplified V_c prediction model. The values of V_{c_L} and V_{c_R} predicted by this VPS configuration during the left engine failure simulation with one set of control inputs, turbulence on and a maximum performance roll to the right is plotted in Figure 6. The MKM needs the first five seconds to find realistic parameter estimates. After that, the predicted V_c settles around 120 knots. This plot shows that the simplified V_c prediction model provides a more stable V_c prediction for the Fokker 50 than the V_c prediction model of the Piper Seneca VPS. Also, the mean V_c prediction error of 5.2 meters per second is better than the V_c prediction errors us-

ing Koolstra's V_c prediction model from Table 7b, but still twice as large as the smallest mean V_c prediction error for the Piper Seneca from Table 7a.

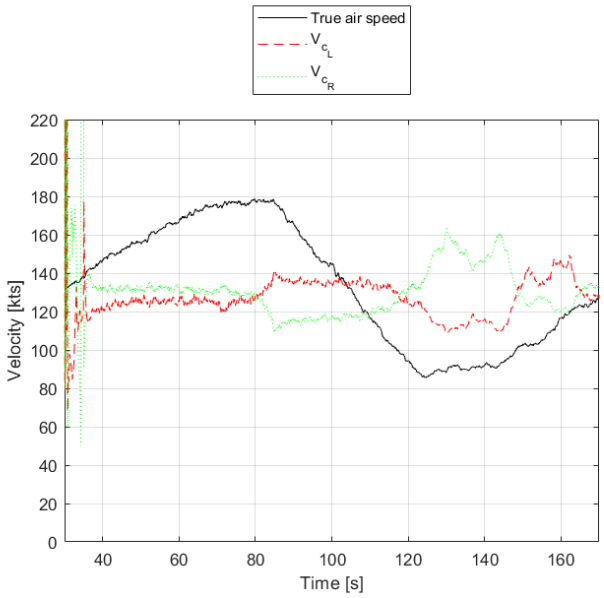

Figure 6: Predicted V_{c_L} and V_{c_R} during the left engine failure simulation with one set of control inputs, turbulence on and a maximum performance roll to the right using the basic model, the MKM and the simplified V_c prediction model.

6 Discussion

The final step in the sensitivity analysis is to discuss what the results from the redesign of the Fokker 50 VPS mean for the sensitivity of the VPS to a change in aircraft dynamics and simulation model complexity. Since the VPS consists of three components, the sensitivity of each of these components is discussed separately below. It should be noted that this discussion is only based on two data points; the Piper Seneca VPS design and the Fokker 50 VPS design.

In Section 4.2 it was found that both the Piper Seneca and the Fokker 50 favor the basic linear model. The basic linear model is able to accurately predict the roll rate of both the Piper Seneca and the Fokker 50 during a maximum performance roll. Even though the used Fokker 50 simulation model is more complex than the Piper Seneca simulation model, adding additional terms did not improve the prediction accuracy but led to over-fitting. The linear model of the VPS is therefore not sensitive to a change in aircraft dynamics and simulation model complexity.

The four parameter estimation methods showed similar V_c prediction errors for the Fokker 50 when they were used in combination with Koolstra's V_c prediction model in Table 7b. The same is true for the V_c prediction errors of the Piper Seneca in Table 7a. Comparing these two tables shows that the relative differences between the four parameter estimation methods are small for both aircraft. When these four parameter estimation methods were combined with the simplified V_c prediction model however in Table 8, the two forgetting algorithms caused diverging V_c predictions. This means that the simplified V_c prediction model favors parameter estimation methods with covariance matrix resets after failure detection such as RLS and MKM, because they provide stable and steady parameter estimates. This comparison however analyzes the sensitivity of the parameter estimation methods to a change in V_c prediction model. The sensitivity of the parameter estimation method to a change in aircraft dynamics and simulation model complexity is displayed in relative differences in Tables 7a and 7b, and the fact that the MKM was selected for the VPS of both aircraft. The parameter estimation methods are therefore not sensitive to a change in aircraft dynamics and simulation model complexity either.

The V_c prediction model from the Piper Seneca VPS however is very sensitive to a change in aircraft dynamics and simulation model complexity, as it struggled to find a stable and accurate V_c prediction when it was implemented in the Fokker 50 VPS. Especially the corrections in Equations 9 and 10 seemed to suit the dynamics of the Piper Seneca only. Even after deriving a simplified V_c prediction model, the mean V_c prediction error for the Fokker 50 was still more than twice as large as the mean V_c prediction error for the Piper Seneca. This was already expected after analyzing the states and control inputs of the two aircraft in a roll-limited situation in Section 2, but based on only two data points it is uncertain whether this is the only reason for the decrease in V_c prediction accuracy.

7 Conclusion

In this paper the sensitivity of the Piper Seneca VPS design to a change in aircraft dynamics and simulation model complexity has been analyzed using a Fokker 50 simulation model. By repeating Koolstra's VPS design process for the Fokker 50 it was shown that no changes to the linear model are required, since the basic linear model accurately predicts a maximum performance roll for both aircraft. Also, the

MKM was selected for both aircraft, because this parameter estimation method gives the lowest V_c prediction errors. The V_c prediction model is very sensitive to a change in aircraft dynamics and simulation model complexity. Whether this high sensitivity can be attributed to the change in aircraft dynamics, the change in simulation model complexity or both, can not be concluded based on the results from this study. This study has however provided a first indication that the Piper Seneca VPS is not generally applicable to all aircraft types and/or simulation models. It is only a first indication, because this sensitivity analysis is only based on two data points; the Piper Seneca VPS design and the Fokker 50 VPS design.

For further research it is therefore recommended to implement the VPS in the simulation model of another aircraft type, such as a long-range passenger jet or a large transport aircraft. If the results show that the VPS consisting of the basic linear model, the MKM and the simplified V_c prediction model is the optimal VPS configuration for this new aircraft type as well, this would indicate that the simplification of the V_c prediction model has made the VPS more applicable to a wider range of aircraft dynamics. Otherwise it should be investigated which specific dynamic features of an aircraft determine the applicability the V_c prediction model.

Acknowledgements

I would like to express my gratitude towards Ir. O. Stroosma and Dr. ir. A. C. in't Veld from the department of Control and Simulation for sharing their knowledge on flight simulation and flight dynamics, for providing feedback and for allowing me to use their SRS facility. Furthermore, I would like to thank Dr. H. J. Koolstra for inspiring this research and for explaining the results of his research. Finally I would like to thank Ing. D. van Os from Fokker Services for providing the Fokker 50 simulation model and for his continued support for the Fokker 50 simulation model project.

References

[1] C. M. Belcastro and J. V. Foster. Aircraft loss-of-control accident analysis. AIAA Guidance, Navigation, and Control Conference, 2010.

[2] H. J. Koolstra. *Preventing Loss of Aircraft Control: Aiding pilots in manual recovery from roll-limited situations.* PhD thesis, Delft University of Technology, 2017.

[3] Federal Aviation Administration, Department of Transportation. *Electronic Code of Federal Regulations: Title 14 Aeronautics and Space.*

[4] J. A. Mulder, W. H. J. J. van Staveren, J. C. van der Vaart, E. de Weerdt, C. C. de Visser, A. C. in 't Veld, and E. Mooij. Flight dynamics, March 2013. Lecture notes AE3202.

[5] N. van den Bovenkamp, M. van Dijk, and D. Ham. Aerodynamic data base for the fokker f27 mk050. Technical Report L-27-218, Fokker Services BV, mar 2002.

[6] D. Graupe. *Identification of Systems.* Robert E. Krieger Publishing Company, 2nd edition, 1976.

[7] C. Kamali, A. A. Pashilkar, and J. R. Rao. Evaluation of recursive least squares algorithm for parameter estimation in aircraft real time applications. *Aerospace Science and Technology*, 15:165–174, 2011.

[8] D. Q. Mayne. Optimal non-stationary estimation of the parameters of a linear system with gaussian inputs. *Journal of Electronics and Control*, 14(1):101–112, 1963.

[9] J. R. Raol, G. Girija, and J. Singh. *Modelling and Parameter Estimation of Dynamic Systems.* Control, Robotics and Sensors. The Institution of Engineering and Technology, 2004.

[10] Anon. Flying qualities of piloted aircraft. Technical report, Department of Defense, 1997.

[11] D. M. Allen. The relationship between variable selection and data augmentation and a method for prediction. *Technometrics*, 16(1):125 – 127, 1974.

[12] J. Stewart. *Calculus Early Trancendentals.* Brooks/Cole, 7th edition, 2012.

A

Aerodynamic and control coefficients

Solving the non-dimensional equations of motion in Section 2.2 of the paper requires the values of the lateral aerodynamic and control coefficients of the Fokker 50. They are determined from the data tables documented in [2]. These data tables have been generated by Fokker through wind tunnel experiments and flight tests. The C_Y, C_l and C_n coefficients are listed in Tables A.1a, A.1b and A.1c along with their corresponding values. These tables also show the names of the data tables and the figure numbers in [2] from which the coefficients were determined. Ranges for which the coefficients are valid and the conditions at which the data tables were generated are listed as well.

Coefficient	Value	Valid range	Conditions	Table name	Figure number
$C_{Y_{\beta_{TO}}}$	-0.3645	-20 <= β <= 20 deg	δ_f = 0 deg α = 2.7 deg	CYTODB	7.1.1 a
$C_{Y_{\beta_T}}$	-0.6356	-20 <= β <= 20 deg	δ_f = 0 deg α = 2.7 deg	CYTDB	7.1.3 a
$C_{Y_{\delta a_L}}$	0	-	-	-	-
$C_{Y_{\delta a_R}}$	0	-	-	-	-
$C_{Y_{\delta_r}}$	0.2762	-20 <= δ_r <= 20 deg	δ_f = 0 deg α = 3 deg	CYDR	7.1.12
$C_{Y_{C_{T_L}}}$	0.0122	-10 <= β <= 10 deg	δ_f = 0 deg α = 12 deg	CYDTCL	7.1.7 b
$C_{Y_{C_{T_R}}}$	-0.0200	-10 <= β <= 10 deg	δ_f = 0 deg α = 12 deg	CYDTCR	7.1.8 b

(a) C_Y coefficients.

Coefficient	Value	Valid range	Conditions	Table name	Figure number
$C_{l_{\beta_{TO}}}$	-0.0643	-20 <= β <= 20 deg	δ_f = 0 deg α = 2.7 deg	CRTODB	7.3.1 a
$C_{l_{\beta_T}}$	-0.0422	-20 <= β <= 20 deg	δ_f = 0 deg α = 2.7 deg	CRTDB	7.3.3 a
$C_{l_{\delta a_L}}$	0.0647	-33 <= δa_L <= 22 deg	α = 7 deg	CRDDAL	7.3.8 a
$C_{l_{\delta a_R}}$	-0.0647	-33 <= δa_R <= 22 deg	α = 8 deg	CRDDAR	7.3.8 b
$C_{l_{\delta_r}}$	0.0195	-20 <= δ_r <= 20 deg	δ_f = 0 deg α = 3 deg	CRDR	7.3.10
$C_{l_{C_{T_L}}}$	0.0018	-10 <= β <= 10 deg	δ_f = 0 deg α = 8.7 deg	CRDTCL	7.3.6 b
$C_{l_{C_{T_R}}}$	-0.0035	-10 <= β <= 10 deg	δ_f = 0 deg α = 8.7 deg	CRDTCR	7.3.7 b

(b) C_l coefficients.

Coefficient	Value	Valid range	Conditions	Table name	Figure number
$C_{n_{\beta_{TO}}}$	-0.0511	-20 <= β <= 20 deg	δ_f = 0 deg α = 2.7 deg	CNTODB	7.2.1 a
$C_{n_{\beta_T}}$	0.1763	-20 <= β <= 20 deg	δ_f = 0 deg α = 2.7 deg	CNTDB	7.2.3 a
$C_{n_{\delta a_L}}$	-0.0047	-33 <= δa_R <= 22 deg	δ_f = 0 deg α = 8 deg	CNDDAL	7.2.8 a
$C_{n_{\delta a_R}}$	0.0047	-33 <= δa_R <= 22 deg	δ_f = 0 deg α = 8 deg	CNDDAR	7.2.8 c
$C_{n_{\delta_r}}$	-0.1152	-20 <= δ_r <= 20	δ_f = 0 deg α = 3 deg	CNDR	7.2.9
$C_{n_{C_{T_L}}}$	-0.0010	-10 <= β <= 10 deg	δ_f = 0 deg α = 8.7 deg	CNDTCL	7.2.6 b
$C_{n_{C_{T_R}}}$	-0.0025	-10 <= β <= 10 deg	δ_f = 0 deg α = 8.7 deg	CNDTCR	7.2.7 b

(c) C_n coefficients.

Table A.1: Values, ranges and sources of the aerodynamic and control coefficients of the Fokker 50.[2]

B

Engine data

Models of the lateral forces and moments caused by the propeller, the engine inlet and the engine jet stream are required to solve the non-dimensional equations of motion in Section 2.2 of the paper. The Fokker 50 simulation model is used to acquire data on the combined forces and moments generated by the two Pratt & Whitney PW125B turboplants and the six-bladed Dowty Rotol propellers. These data are gathered by doing three runs with the simulation model controlled by a joystick. The first run is a symmetric flight, to serve as a baseline for the other runs. The second and third runs are wings-level sideslipping flights with minimum and maximum rudder input, to investigate the effect of a change in sideslip angle. During these runs gradual variations in flight path angle are applied to obtain data over a large velocity range. The three runs listed above are carried out twice; once with both engines idling and feathered propellers and once with both engines set to full throttle. Since V_{mca} is calculated with the critical engine inoperative, the interesting results are the data of the critical engine with the propeller feathered and the other engine at full throttle. The critical engine of the Fokker 50 is the left engine. Therefore, the results for the left engine inoperative with the propeller feathered and the right engine set to full throttle are shown in Sections B.1 and B.2 respectively.

B.1. Left engine shut and propellers feathered

The values of the thrust coefficients, sideforces, rolling moments and yawing moments of the left engine with the propeller feathered as a function of velocity are shown in Figures B.1a, B.1b, B.1c and B.1d respectively. The data in these plots represent the drag from the feathered propeller and the engine inlet. Two interesting observations are made. The first observation is that the thrust coefficient, the sideforce and the rolling moment are relatively small compared to an engine at full throttle, as shown in the next section. The second observation is that the sideforce largely depends on the sideslip angle as shown in Figure B.1b.

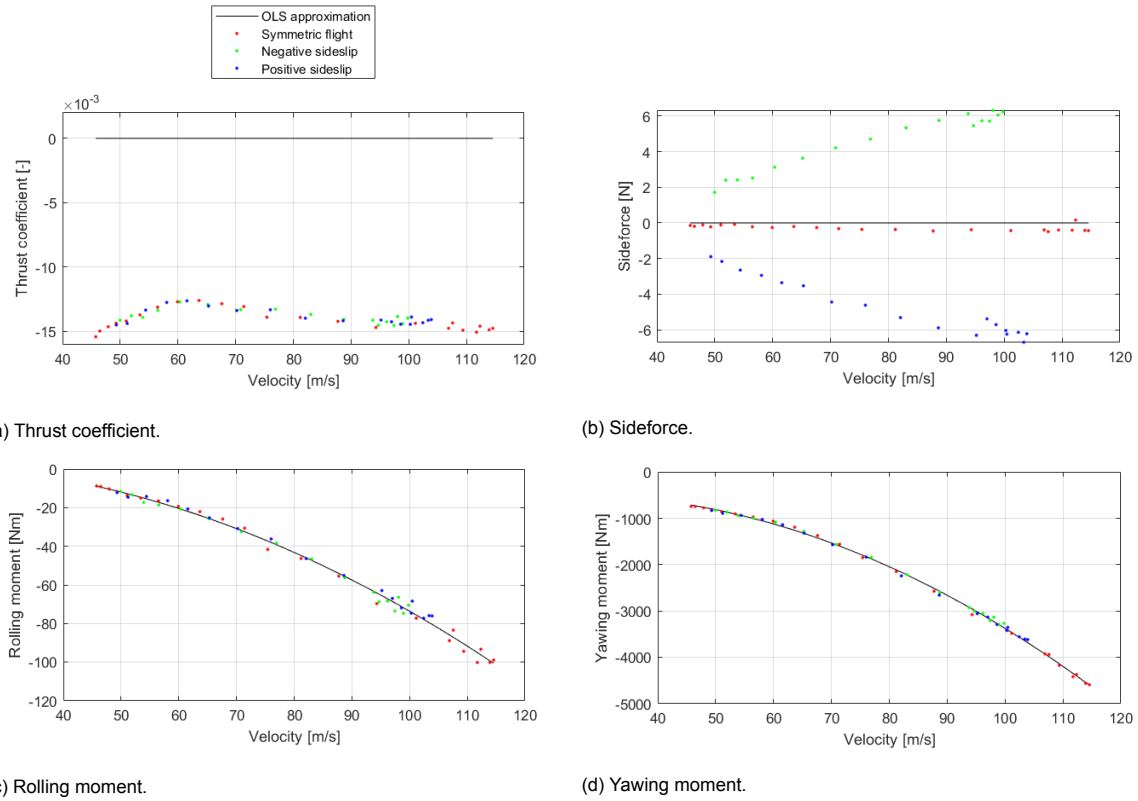

(a) Thrust coefficient.

(b) Sideforce.

(c) Rolling moment.

(d) Yawing moment.

Figure B.1: Forces and moments of the left engine with the propeller feathered caused by the propeller thrust, inlet drag and the engine jet forces excluding slipstream effects on the fuselage and tail.

The data for the left engine with the propeller feathered are used to create models of the thrust coefficient, sideforce, rolling moment and yawing moment as a function of air speed. The thrust coefficient and the sideforce of an engine with the propeller feathered are more than a factor 10 smaller than the thrust coefficient and the sideforce of an engine at full throttle, as shown in the next section. They are therefore considered neglectable, which leads to Equations B.1 to B.2. Aerodynamic drag from the propeller and the engine inlet are the main causes of the rolling moment and yawing moment of the left engine with the propeller feathered. As a result, they follow a second order relation with air speed, which leads to equations B.3 and B.4.

$$C_{T_L} = 0 \tag{B.1}$$
$$Y_{T_L} = 0 \tag{B.2}$$
$$l_{T_L} = 1.74 + 0.21 \cdot V + -9.63 \cdot 10^{-3} \cdot V^2 \tag{B.3}$$
$$n_{T_L} = -806 + 25.4 \cdot V + -0.51 \cdot V^2 \tag{B.4}$$

B.2. Right engine at full throttle

The values of the thrust coefficients, sideforces, rolling moments and yawing moments of the right engine at full throttle as a function of velocity are shown in Figures B.2a, B.2b, B.2c and B.2d respectively. Again, two interesting observations are made. First, the magnitude of the forces and moments are linearly related to velocity. Second, the sideforce largely depends on the sideslip angle as shown in Figure B.2b.

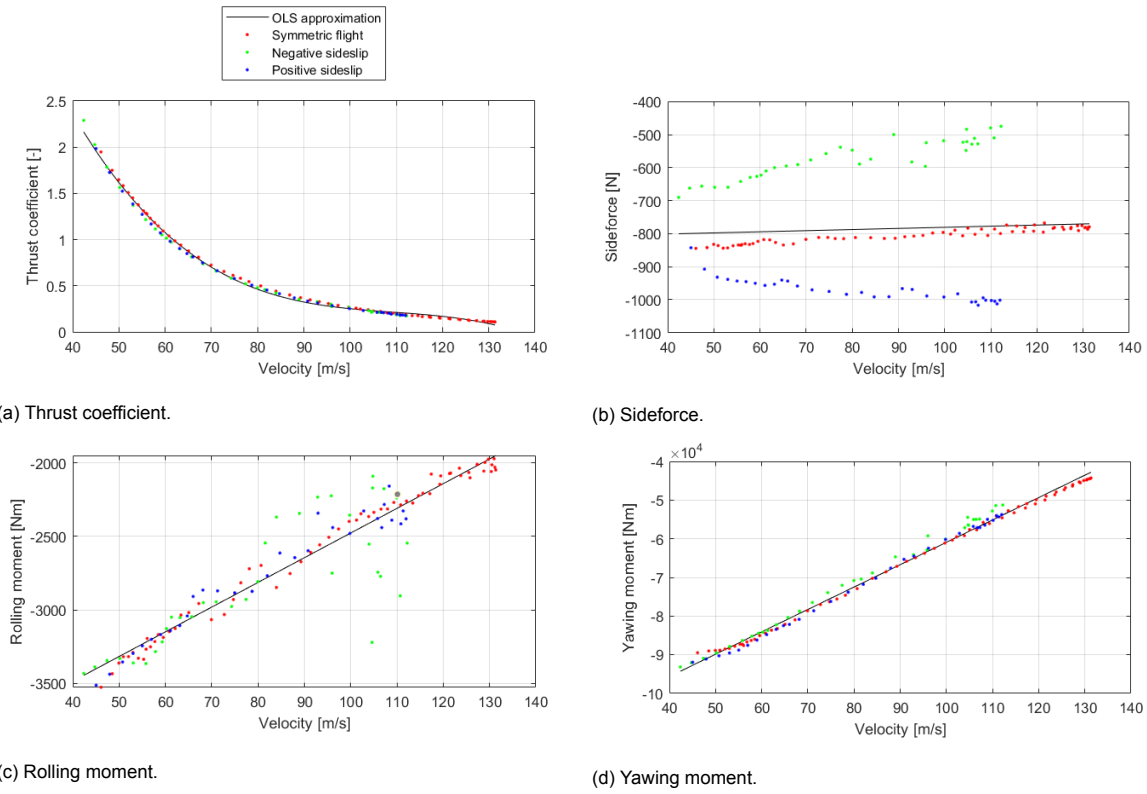

(a) Thrust coefficient.

(b) Sideforce.

(c) Rolling moment.

(d) Yawing moment.

Figure B.2: Forces and moments of the right engine at full throttle caused by the propeller thrust, inlet drag and the engine jet forces excluding slipstream effects on the fuselage and tail.

The data for the right engine at full throttle are used to create models of the thrust coefficient, sideforce, rolling moment and yawing moment as a function of air speed. The effects of sideslip angle are neglected under the assumption that the sideslip angle is small during the determination of V_{mca}. A third order polynomial is fit to the thrust coefficient, leading to Equation B.5. A linear relation is assumed for the forces and moments, leading to Equations B.6, B.7 and B.8.

$$C_{T_R} = 8.05 - 0.21 \cdot V + 1.87 \cdot 10^{-3} \cdot V^2 + -5.70 \cdot 10^{-6} \cdot V^3 \tag{B.5}$$

$$Y_{T_R} = -815 + 0.34 \cdot V \tag{B.6}$$

$$l_{T_R} = -4.16 \cdot 10^3 + 16.8 \cdot V \tag{B.7}$$

$$n_{T_R} = -119 \cdot 10^3 + 580 \cdot V \tag{B.8}$$

C

Zero sideslip scenario

In addition to the analysis of the full rudder deflection scenario in Section 2.2 of the paper, the three lateral non-dimensional equations of motion are solved for the zero sideslip scenario. The reason for this is that even though all the states in Figure 2 are achievable, the section of this plot where the sideslip angle is smaller than zero does not portray a realistic aircraft state. It does not make sense to use a full rudder input in combination with a negative sideslip angle, because there the rudder is effective enough to counteract the yawing moment from the engine, without requiring an additional yawing moment from the weathervane effect of the vertical tail. A more realistic plot is shown in Figure C.1, which combines the solution of the full rudder deflection scenario with the solution of the zero sideslip scenario. The result of the zero sideslip scenario is plotted between the velocity range of 90.4 to 120 knots. It shows how a negative rudder deflection is required to counteract the yawing moment of the right engine and that a positive roll angle counteracts the sideforce of the rudder. It also visualizes how the effectiveness of the aileron and rudder decreases when the velocity decreases. When the rudder limit is hit at 90.4 knots, the required roll angle is slightly smaller than 5 degrees. This means that a small sideslip angle can be induced to generate an additional yawing moment with the vertical tail, while staying below the maximum roll angle of 5 degrees for V_{mca} defined by Federal Aviation Regulations (FAR). This principle is shown by the full rudder deflection scenario, which is plotted between the velocity range of 63.0 to 90.4 knots. It shows how a non-zero sideslip angle is required to counteract the yawing moment from the engine using the additional yawing moment from the weathervane effect of the vertical tail. At 87.9 knots the required roll angle is larger than 5 degrees. This is the point of V_{mca} as defined by FAR. It should be noted that this value should not be compared to the value of V_{mca} of 87.0 knots indicated air speed from the Aircraft Flight Manual (AFM) of the Fokker 50. That value was determined for a flap setting of 5 degrees, while this numerical solution was determined for a flap setting of 0 degrees.

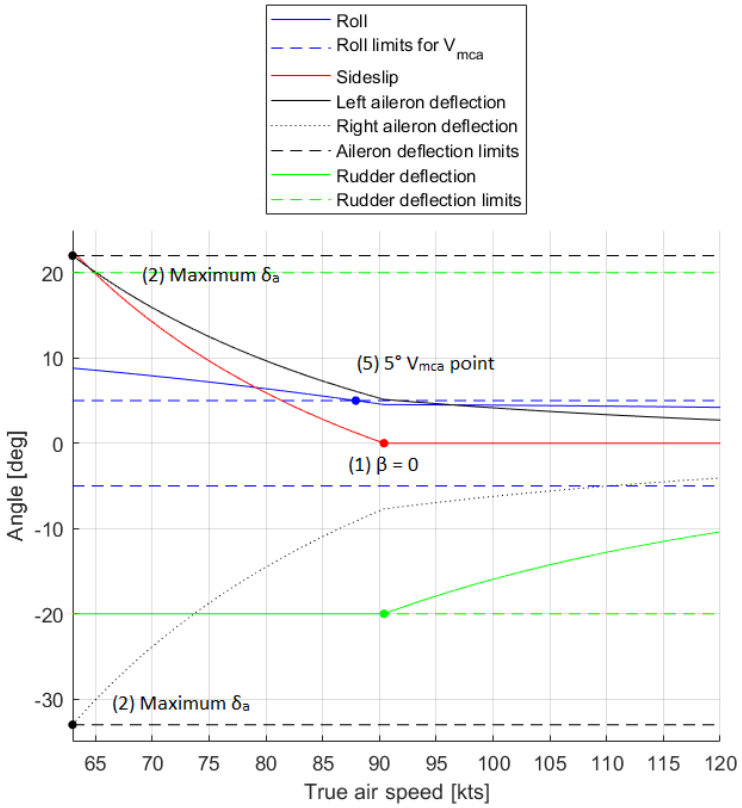

Figure C.1: Numerically determined roll angle, sideslip angle and control surface deflections of the Fokker 50 during straight and level flight with the left engine inoperative and the propeller feathered and the right engine at full throttle.

D

Autopilot

An autopilot is designed from scratch to control the trajectory of the Fokker 50 during the simulations in Section 4.1 of the paper. The original Fokker 50 simulation model contains feedback loops for pitch hold, altitude hold and roll angle hold modes, but it is not capable of tracking a trajectory. Therefore this newly designed autopilot can track velocity, heading, altitude and sideslip reference signals using the controllers depicted in Sections D.1, D.2, D.3 and D.4 respectively.

D.1. Velocity controller

The velocity is controlled by the velocity controller depicted in Figure D.1, which generates a reference angle for the throttle levers from the measured velocity. The controller consists of a single feedback loop with PID gains. Their values are listed in Table D.1. The differentiator is used to make the transient response of the engines more aggressive, while the integrator is used to amplify any steady state velocity errors.

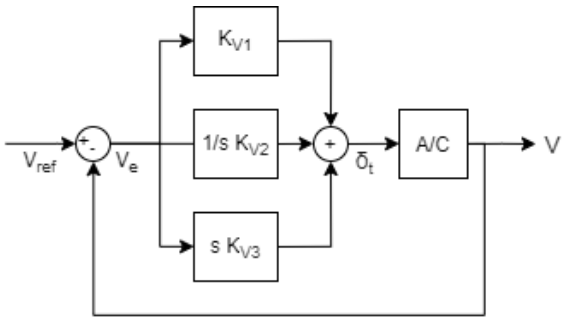

Figure D.1: Diagram of the velocity controller, which generates a throttle lever angle command from the measured velocity.

Gain	Value
K_{V_1}	0.1
K_{V_2}	0.01
K_{V_3}	0.05

Table D.1: Gains of the velocity controller.

D.2. Heading controller

The heading is controlled by the heading controller depicted in Figure D.2, which generates an aileron deflection command from the measured roll rate, roll angle and heading angle. The controller consists of three nested feedback loops. The two inner loops have proportional gains. The outer loop which

controls the heading has a more complex PID controller with the gains listed in Table D.2. The differentiator gain is relatively large compared to the proportional gain to avoid dangerously large bank angles during large heading reference errors. For the same reason the integrator gain is kept relatively small, even though steady state heading errors are difficult to eliminate.

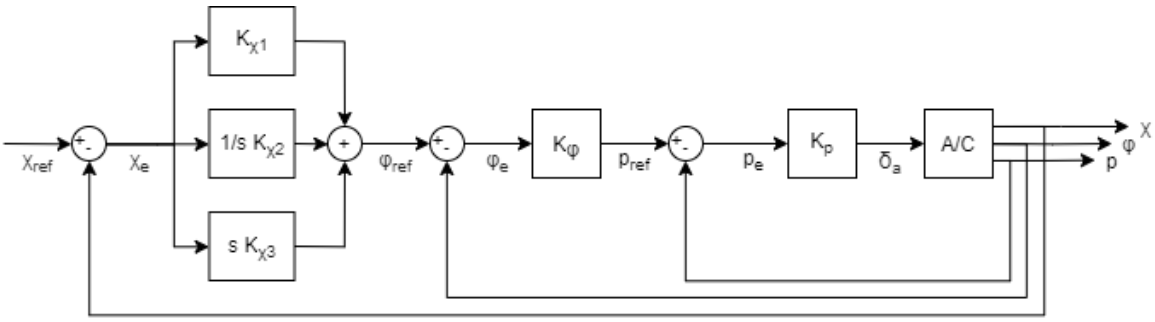

Figure D.2: Diagram of the heading controller, which generates an aileron deflection command from the measured roll rate, roll angle and heading angle.

Gain	Value
K_p	-3.0
K_ϕ	1.0
K_{χ_1}	1.0
K_{χ_2}	0.15
K_{χ_3}	1.0

Table D.2: Gains of the heading controller.

D.3. Altitude controller

The altitude is controlled by the altitude controller depicted in Figure D.3, which generates an elevator deflection command from the measured pitch rate, pitch angle and altitude. The controller consists of three nested feedback loops. The two inner loops have proportional gains. The outer loop which controls the altitude has a more complex PID controller with the gains listed in Table D.3. Each of the PID gains are relatively small, because large linear control gains can pull the aircraft into a stall during large altitude reference errors.

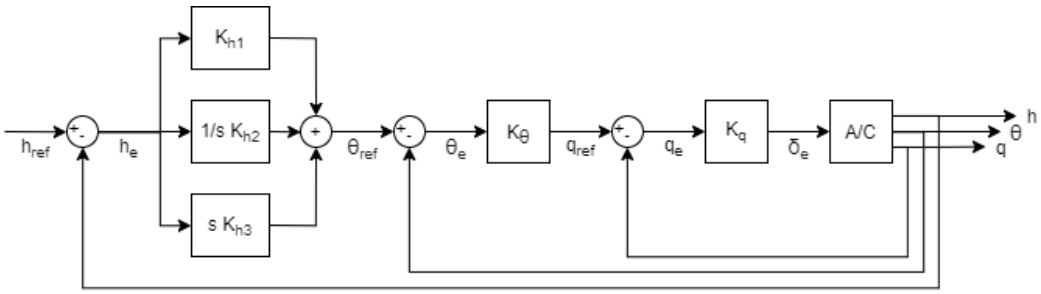

Figure D.3: Diagram of the altitude controller, which generates an elevator deflection command from the measured pitch rate, pitch angle and altitude.

Gain	Value
K_q	-3.0
K_θ	1.0
K_{h_1}	0.01
K_{h_2}	0.002
K_{h_3}	0.003

Table D.3: Gains of the altitude controller.

D.4. Sideslip controller

The sideslip angle is controlled by the sideslip controller depicted in Figure D.4, which generates a rudder deflection command from the measured yaw rate and sideslip angle. The controller consists of two nested feedback loops. The inner loop has a proportional gain. The outer loop which controls the sideslip angle has a PI controller with the gains listed in Table D.4. Under normal operation a simple proportional controller would suffice, but for special circumstances such as asymmetric thrust an integrator is needed to reduce the steady-state sideslip error.

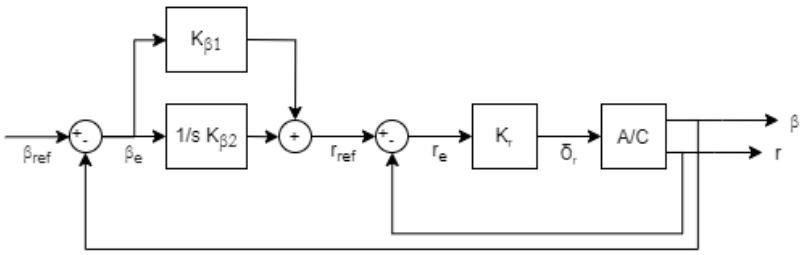

Figure D.4: Diagram of the sideslip controller, which generates a rudder deflection command from the measured yaw rate and sideslip angle.

Gain	Value
K_r	-3.0
K_{β_1}	-1.5
K_{β_2}	-0.7

Table D.4: Gains of the sideslip controller.

E

Raw V_c prediction data

Tables 7b and 8 of the paper present the means and standard deviations of the V_c prediction errors. In this appendix the raw data which were used to compute the means for the VPS configurations with the basic model are presented. Tables E.2 and E.3 show the raw data corresponding to Tables 7b and 8 in the paper, but first the mean V_c prediction errors per failure are listed in Tables E.1a and E.1b.

Failure	Mean prediction error [m/s]
No failure	14.4
50% loss of aileron	17.1
100% loss of rudder	2.9
Left engine failure	11.5
Right engine failure	9.8
Asymmetry left wing heavy	14.4
Asymmetry right wing heavy	15.4
Rudder hardover to the left	19.9
Rudder hardover to the right	30.4

(a) Combination of the basic model, the MKM and Koolstra's V_c prediction model.

Failure	Mean prediction error [m/s]
No failure	6.7
50% loss of aileron	13.3
100% loss of rudder	1.8
Left engine failure	2.3
Right engine failure	3.1
Asymmetry left wing heavy	5.3
Asymmetry right wing heavy	3.4
Rudder hardover to the left	1.6
Rudder hardover to the right	2.9

(b) Combination of the basic model, the MKM and the simplified V_c prediction model.

Table E.1: Mean V_c prediction errors per failure for the Fokker 50.

#	Failure	Inputs	Turb.	Roll	RLS	FAD	MKM	FA
1	No failure	1	No	Left	-11.3	0.3	15.1	15.1
2	No failure	1	No	Right	-11.2	0.3	15.1	15.1
3	No failure	1	Yes	Left	9.6	-36.7	15.5	12.5
4	No failure	1	Yes	Right	10.0	-34.4	8.9	7.3
5	No failure	2	No	Left	15.1	4.6	15.2	15.2
6	No failure	2	No	Right	15.0	3.6	15.2	15.2
7	No failure	2	Yes	Left	14.4	1.2	14.4	14.4
8	No failure	2	Yes	Right	15.5	6.5	15.5	9.2
9	50% loss of aileron	1	No	Left	-9.0	1.3	-20.1	15.1
10	50% loss of aileron	1	No	Right	5.8	-0.5	-2.9	15.1
11	50% loss of aileron	1	Yes	Left	15.3	-33.9	15.3	10.0
12	50% loss of aileron	1	Yes	Right	3.7	-36.3	-22.7	2.2
13	50% loss of aileron	2	No	Left	15.1	-36.8	15.1	-10.1
14	50% loss of aileron	2	No	Right	15.1	-36.9	-9.5	15.1
15	50% loss of aileron	2	Yes	Left	14.9	-38.3	-38.3	14.9
16	50% loss of aileron	2	Yes	Right	14.0	-37.4	-12.5	14.0
17	100% loss of rudder	1	No	Left	8.2	0.3	5.3	15.2
18	100% loss of rudder	1	No	Right	5.0	0.2	1.1	15.1
19	100% loss of rudder	1	Yes	Left	11.1	-0.7	6.5	13.9
20	100% loss of rudder	1	Yes	Right	5.8	0.4	0.3	14.8
21	100% loss of rudder	2	No	Left	7.6	0.8	5.3	15.2
22	100% loss of rudder	2	No	Right	4.2	0.6	0.8	15.1
23	100% loss of rudder	2	Yes	Left	7.0	1.0	1.9	15.3
24	100% loss of rudder	2	Yes	Right	7.4	1.5	2.1	14.7
25	Left engine	1	No	Right	-5.9	0.5	15.0	-36.6
26	Left engine	1	Yes	Right	14.0	-0.2	-12.4	-31.2
27	Left engine	2	No	Right	-15.1	-1.4	15.0	11.9
28	Left engine	2	Yes	Right	15.6	-20.6	15.6	15.6
29	Right engine	1	No	Left	-18.2	0.2	15.0	-1.0
30	Right engine	1	Yes	Left	16.3	1.8	4.5	16.3
31	Right engine	2	No	Left	15.0	0.4	8.9	12.3
32	Right engine	2	Yes	Left	15.1	-37.9	11.0	15.0
33	Asymmetry left	1	No	Right	11.1	0.2	15.1	3.6
34	Asymmetry left	1	Yes	Right	14.4	-0.6	14.4	8.8
35	Asymmetry left	2	No	Right	15.2	0.5	15.2	4.5
36	Asymmetry left	2	Yes	Right	13.0	-1.7	13.0	3.4
37	Asymmetry right	1	No	Left	7.1	0.3	-0.1	1.0
38	Asymmetry right	1	Yes	Left	8.1	-36.6	15.2	3.7
39	Asymmetry right	2	No	Left	11.8	0.6	-36.2	1.0
40	Asymmetry right	2	Yes	Left	13.6	2.4	10.1	0.4
41	Rudder hardover left	1	No	Right	-14.3	0.3	-22.7	1.2
42	Rudder hardover left	1	Yes	Right	-15.6	0.1	-19.4	1.4
43	Rudder hardover left	2	No	Right	-14.9	0.3	-19.8	-5.1
44	Rudder hardover left	2	Yes	Right	-7.2	0.8	-17.6	0.7
45	Rudder hardover right	1	No	Left	15.0	-36.8	-36.8	0.7
46	Rudder hardover right	1	Yes	Left	5.3	0.1	13.3	-0.5
47	Rudder hardover right	2	No	Left	14.9	-0.8	-36.8	-0.2
48	Rudder hardover right	2	Yes	Left	15.0	-1.0	-34.9	-7.6

Table E.2: V_c prediction errors for each simulation using the basic linear model and Koolstra's V_c prediction model.

#	Failure	Inputs	Turb.	Roll	RLS	FAD	MKM	FA
1	No failure	1	No	Left	16.3	154.2	8.9	238.3
2	No failure	1	No	Right	17.2	156.0	9.9	238.3
3	No failure	1	Yes	Left	10.5	238.3	5.8	138.6
4	No failure	1	Yes	Right	13.1	240.6	4.7	80.4
5	No failure	2	No	Left	12.0	238.2	7.7	238.2
6	No failure	2	No	Right	12.3	238.2	6.4	238.2
7	No failure	2	Yes	Left	14.0	237.9	3.6	40.1
8	No failure	2	Yes	Right	16.0	239.0	6.8	62.7
9	50% loss of aileron	1	No	Left	36.9	238.2	28.8	238.2
10	50% loss of aileron	1	No	Right	22.4	238.2	12.7	238.2
11	50% loss of aileron	1	Yes	Left	51.0	241.1	18.9	86.4
12	50% loss of aileron	1	Yes	Right	5.8	238.7	-1.1	31.8
13	50% loss of aileron	2	No	Left	28.3	238.2	15.5	238.2
14	50% loss of aileron	2	No	Right	15.2	238.1	3.9	238.1
15	50% loss of aileron	2	Yes	Left	16.6	236.7	23.8	60.5
16	50% loss of aileron	2	Yes	Right	5.7	237.6	-1.9	76.4
17	100% loss of rudder	1	No	Left	9.4	35.8	2.6	72.7
18	100% loss of rudder	1	No	Right	5.9	32.4	-1.1	66.1
19	100% loss of rudder	1	Yes	Left	14.0	120.8	3.4	43.6
20	100% loss of rudder	1	Yes	Right	7.7	97.7	-1.7	53.7
21	100% loss of rudder	2	No	Left	8.1	36.5	2.7	53.7
22	100% loss of rudder	2	No	Right	4.5	36.3	-1.1	32.4
23	100% loss of rudder	2	Yes	Left	8.4	238.0	-0.5	31.4
24	100% loss of rudder	2	Yes	Right	8.3	146.8	-1.2	33.1
25	Left engine	1	No	Right	24.2	238.4	2.3	31.7
26	Left engine	1	Yes	Right	82.4	165.8	2.5	234.0
27	Left engine	2	No	Right	21.9	238.4	1.5	91.1
28	Left engine	2	Yes	Right	17.9	237.6	2.9	23.9
29	Right engine	1	No	Left	8.4	229.0	3.2	238.4
30	Right engine	1	Yes	Left	10.2	239.9	3.3	239.9
31	Right engine	2	No	Left	9.4	92.9	3.5	35.8
32	Right engine	2	Yes	Left	8.0	35.5	2.3	30.1
33	Asymmetry left	1	No	Right	30.1	62.6	4.9	99.7
34	Asymmetry left	1	Yes	Right	26.0	42.1	6.3	70.7
35	Asymmetry left	2	No	Right	21.5	54.3	2.7	28.6
36	Asymmetry left	2	Yes	Right	15.1	42.4	7.2	18.8
37	Asymmetry right	1	No	Left	24.3	238.3	-0.4	77.1
38	Asymmetry right	1	Yes	Left	18.2	238.4	9.9	79.4
39	Asymmetry right	2	No	Left	19.3	238.2	3.1	55.7
40	Asymmetry right	2	Yes	Left	10.7	240.1	-0.4	15.4
41	Rudder hardover left	1	No	Right	6.7	41.8	2.0	90.0
42	Rudder hardover left	1	Yes	Right	4.2	54.6	1.9	92.9
43	Rudder hardover left	2	No	Right	5.6	21.8	2.3	2.8
44	Rudder hardover left	2	Yes	Right	7.7	25.8	0.0	26.4
45	Rudder hardover right	1	No	Left	7.7	62.5	3.5	58.0
46	Rudder hardover right	1	Yes	Left	4.2	45.1	-0.2	3.1
47	Rudder hardover right	2	No	Left	6.5	23.3	3.8	18.7
48	Rudder hardover right	2	Yes	Left	6.7	26.6	4.3	68.1

Table E.3: V_c prediction errors for each simulation using the basic linear model and the simplified V_c prediction model.

F

Cockpit displays

At the start of this project the outputs of the Fokker 50 simulation model were displayed to the pilots through the two standard instrument panels that were originally built for the Cessna Citation simulation model. These instrument panels had a different configuration than the instrument panels of a Fokker 50 cockpit, and they were not capable of displaying all the outputs of the Fokker 50 simulation model. To increase physical fidelity, the two main instrument panels of the Fokker 50, the primary flight display and the engine display, were rebuilt in C++ using OpenGL based on instrument system descriptions in the Aircraft Operating Manual of the Fokker 50.[1] They are shown in Figures F.1 and F.2. Especially for this project a sideslip indicator is added to the PFD, which is mainly used to accurately present the sideslip angle during asymmetric thrust conditions.

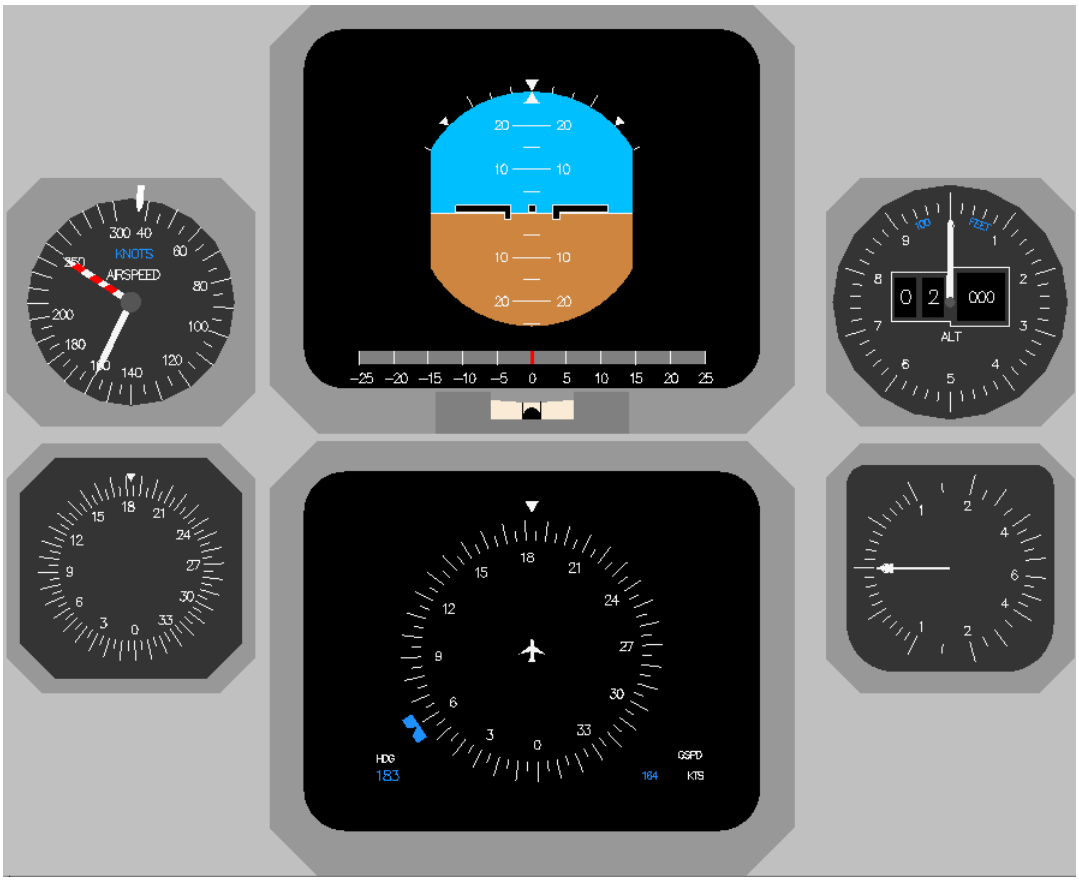

Figure F.1: Primary flight display of the Fokker 50 including an added sideslip indicator.

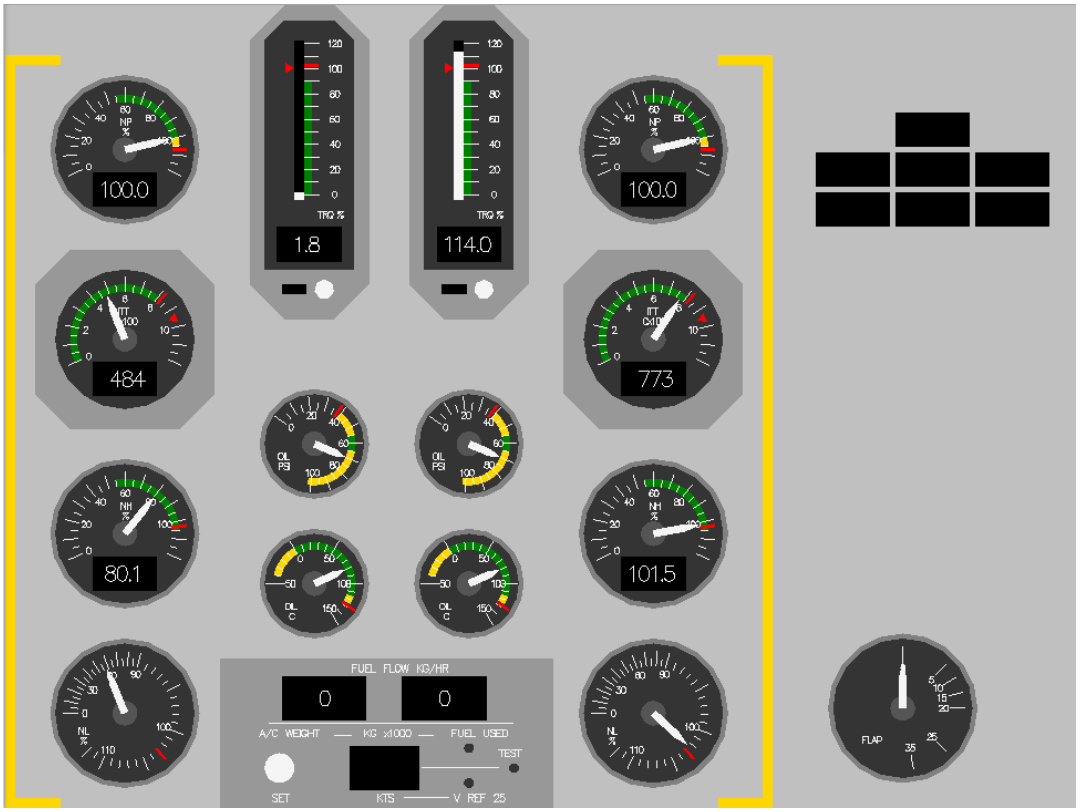

Figure F.2: Engine display of the Fokker 50.

G

Status Fokker 50 simulation model

The Fokker 50 simulation model that was used for this study is still a work in progress. Therefore the following four tasks still need to be carried out after this project.

- A few ADA files still need to be implemented in C++. Figure G.1 shows the files which have already been implemented in green, the files which have been partially implemented in orange and the files which have not been implemented in red. The most important files which still need to be implemented are the windfields and microbursts in the 'Atmosphere' block, the 'scheduler__stop.a' file in 'Host main' block, and the files in the 'Forward main' block which need to be combined with the Control Loading System files of the SRS Control Loading module that read the QFeel channel.
- All properties of the classes in each header file should be made private instead of public. When the ADA files were converted to C++, there was the problem that in ADA a class property can have the same name as a class method, while this is not possible in C++. The original Fokker 50 simulation model in ADA contains many public class methods which return the value of a private class property, to give other objects read access to these private class properties. The package 'AIRCRAFT_MOTION' defined in the ADA file 'acft_mot_b.a' for example, contains a public class method named 'euler_angles()', which returns the value of the private class property 'euler_angles'. To solve the conversion problem to C++, such public class methods were removed and the corresponding private class property was made public in the C++ header file. The danger of this is that it gives other objects read and write access to these class properties, instead of read access only. Therefore it would be better to make the class property 'euler_angles' private again, to implement the public class method 'euler_angles()' with a different name such as 'get_euler_angles()', and to change the instances in other classes in which this method is called from 'euler_angles' to 'get_euler_angles()'.
- The feedback forces which the 'FCS Adapter' module sends to the QFeel channel need to be read by the Control Loading System of the SRS Control Loading module. Currently control loading is simulated by linear springs, and elevator trimming is done by moving the elevator itself instead of the elevator trim tab in the 'FCS Adapter'. When the Control Loading Module of the SRS reads the force offsets and gradients from the qfeel channel, the aerodynamic forces on the control system will feel more realistic and longitudinal trimming can be done with the elevator trim tab instead of the elevator.
- Even though the original simulation model of the Fokker 50 has been validated by Fokker Aircraft, the simulation model in DUECA still needs to be verified to confirm that no conversion errors have been made.

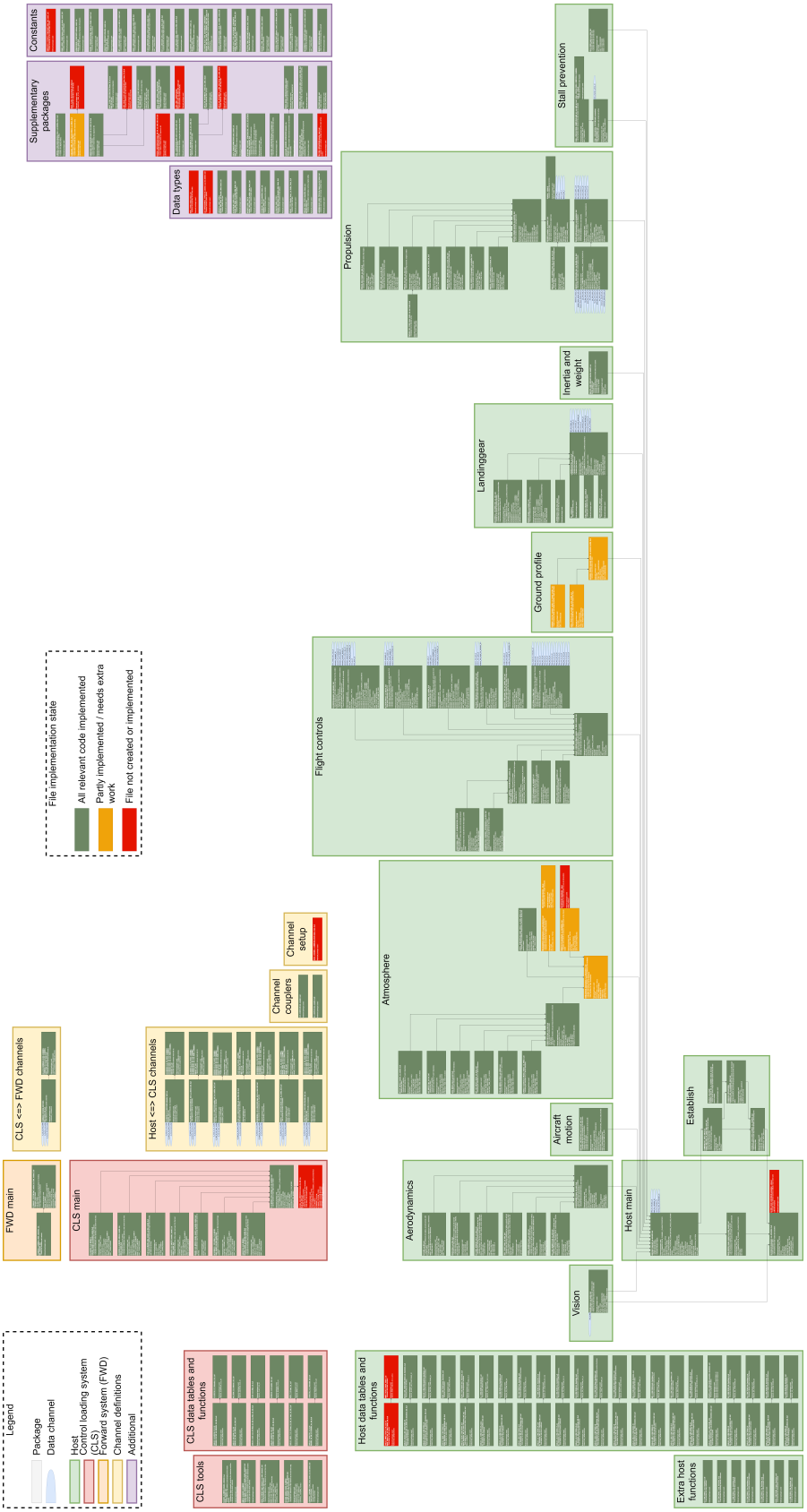

Figure G.1: Implemented files of the Fokker 50 simulation model.

Bibliography

[1] *Aircraft Operating Manual Fokker 50*. Fokker, January 2018. Version 70 Issue 021.

[2] N. van den Bovenkamp, M. van Dijk, and D. Ham. Aerodynamic data base for the fokker f27 mk050. Technical Report L-27-218, Fokker Services BV, March 2002.